FINAL REPORT

Impacts of Enhanced Reductive Bioremediation on Post-Remediation Groundwater Quality

SERDP Project ER-2131

NOVEMBER 2015

Robert C. Borden
Jason M. Tillotson
North Carolina State University

Gene-Hua Crystal Ng
Barbara A. Bekins
Douglas B. Kent
U.S. Geological Survey

SERDP
DOD ▪ EPA ▪ DOE

REPORT DOCUMENTATION PAGE

1. REPORT DATE *(DD-MM-YYYY)* 15-11-2015	2. REPORT TYPE Technical Report	3. DATES COVERED *(From - To)* March 2011 – March 2015

4. TITLE AND SUBTITLE	5a. CONTRACT NUMBER W912HW-11-C-0058
Impacts of Enhanced Reductive Bioremediation on Post- Remediation Groundwater Quality	5b. GRANT NUMBER ER-2131
	5c. PROGRAM ELEMENT NUMBER

6. AUTHOR(S)	5d. PROJECT NUMBER
Borden, Robert C. Tillotson, Jason M. Ng, Gene-Hua Crystal Bekins, Barbara A. Kent, Douglas B.	5e. TASK NUMBER
	5f. WORK UNIT NUMBER

7. PERFORMING ORGANIZATION NAME(S) AND ADDRESS(ES) North Carolina State Univ. U. S. Geological Survey 2711 Founders Dr. 345 Middlefield Rd Raleigh, NC 27695 Menlo Park, CA 94025	8. PERFORMING ORGANIZATION REPORT NUMBER

9. SPONSORING / MONITORING AGENCY NAME(S) AND ADDRESS(ES) Strategic Environmental Research and Development Program 4800 Mark Center Drive, Suite 17D08, Alexandria, VA 22350	10. SPONSOR/MONITOR'S ACRONYM(S) SERDP
	11. SPONSOR/MONITOR'S REPORT NUMBER(S)

12. DISTRIBUTION / AVAILABILITY STATEMENT

Unlimited Distribution

13. SUPPLEMENTARY NOTES

14. ABSTRACT

Electron donor (ED) addition can be very effective in stimulating enhanced reductive bioremediation (ERB) of a wide variety of groundwater contaminants. However, ERB can result in Secondary Water Quality Impacts (SWQIs) including decreased levels of dissolved oxygen, nitrate, and sulfate, and elevated levels of dissolved manganese, dissolved iron, methane, sulfide, organic carbon, and naturally occurring hazardous compounds (e.g., arsenic). Fortunately, this 'plume' of impacted groundwater is usually confined within the original contaminant plume and is unlikely to adversely impact potable water supplies. This report presents the results of research performed on this topic as part of project ER-2131 "Numerical Modeling of Post-Remediation Impacts of Anaerobic Bioremediation on Groundwater Quality".

15. SUBJECT TERMS
secondary water quality impacts; anaerobic bioremediation; enhanced reductive dechlorination; methane; iron; manganese; arsenic

16. SECURITY CLASSIFICATION OF:			17. LIMITATION OF ABSTRACT	18. NUMBER OF PAGES	19a. NAME OF RESPONSIBLE PERSON Robert C. Borden
a. REPORT unclassified	b. ABSTRACT unclassified	c. THIS PAGE unclassified	UU		19b. TELEPHONE NUMBER *(include area code)* 919-873-1060

TABLE OF CONTENTS

LIST OF FIGURES

LIST OF TABLES

ACRONYMS AND ABBREVIATIONS

μmol/g	micromoles per gram
g/kg	grams per kilogram
keq	kiloequivalents
m	meter
m/d	meters per day
m/yr	meters per year
mg/kg	milligrams per kilogram
mg/L	milligrams per liter
mM	millimoles per liter
AFCEE	Air Force Center for Environmental Excellence
AFCEC	Air Force Civil Engineering Center
am-Fe(OH)$_3$	Amorphous Ferrihydrite
AMO	Anaerobic Methane Oxidation
As	Arsenic
As[III]	Arsenic[III]
As[V]	Arsenic[V]
B	Boron
BEX	Benzene, Ethylbenzene, and Xylene
BMSOC	Biogenic, Mixed-Stoichiometry Organic Carbon
C_6H_6	Benzene
CEC	Cation Exchange Capacity
CH_4	Methane
ClO_4^-	Perchlorate
CO_2	Carbon Dioxide
COCs	Contaminants of Concern
Cr[III]	Chromium[III] (Trivalent Chromium)
Cr[VI]	Chromum[VI] (Hexavalent Chromium)
1,1-DCE	1,1-Dichloroethene
cis-1,2-DCE	*cis*-1,2-Dichloroethene
trans-1,2-DCE	*trans*-1,2-Dichloroethene
DIC	Dissolved Inorganic Carbon
DOC	Dissolved Organic Carbon
DOD	Department of Defense
e^-	electron
ED	Electron Donor
ERB	Enhanced Reductive Bioremediation
ESTCP	Environmental Security Technology Certification Program
EVO	Emulsified Vegetable Oil
Fe	Iron
Fe[II]	Iron[II] (Ferrous Iron)
Fe[III]	Iron[III] (Ferric Iron)
Fe^{2+}	Dissolved Iron
$FeCO_3$	Siderite

FeOOH	Goethite
H^+	Hydrogen Ion
H_2	Hydrogen
H_2CO_3	Carbonic Acid
H_2S	Hydrogen Sulfide
HCl	Hydrochloric Acid
HMX	High Melting Explosive ($C_4H_8N_8O_8$)
MCL	Maximum Contamination Limit
Mn	Manganese
Mn[II]	Manganese[II]
Mn[IV]	Manganese[IV]
Mn^{2+}	Dissolved Manganese
$MnCO_3$	Rhodochrosite
N_2	Nitrogen
NCSU	North Carolina State University
NFESC	Naval Facilities Engineering Service Center
NO_3^-	Nitrate
NVDOC	Non-Volatile Dissolved Organic Carbon
O_2	Dissolved Oxygen
OH^-	Hydroxide Ion
ORP	Oxidation-Reduction Potential
PCE	Tetrachloroethene
PE	Partial Equilibrium
pK_{SP}	Solubility Product Constant
PHT3D	A reactive multicomponent transport model for saturated porous media
PRB	Permeable Reactive Barrier
RDX	Research Department Formula X ($C_3H_6N_6O_6$)
S^{2-}	Sulfide
SERDP	Strategic Environmental Research and Development Program
SO_4^{2-}	Sulfate
SQWI	Secondary Water Quality Impact
SU	Standard Units (for pH)
TCE	Trichloroethene
TcO_4^-	Pertechnetate
TEA	Terminal Electron Acceptor
TEAP	Terminal Electron Accepting Process
TNT	Trinitrotoluene
TOC	Total Organic Carbon
U[IV]	Uranium[IV] (Tetravalent Uranium)
U[VI]	Uranium[VI] (Hexavalent Uranium)
UO_2^{2+}	Uranyl Ion
USAF	United States Air Force
USEPA	United States Environmental Protection Agency
USGS	United States Geological Survey
VFA	Volatile Fatty Acid

ACKNOWLEDGEMENTS

EXECUTIVE SUMMARY

Electron donor (ED) addition can be very effective in stimulating enhanced reductive bioremediation (ERB) of a wide variety of groundwater contaminants. However, ERB can result in Secondary Water Quality Impacts (SWQIs) including decreased levels of dissolved oxygen (O_2), nitrate (NO_3^-), and sulfate (SO_4^{2-}), and elevated levels of dissolved manganese (Mn^{2+}), dissolved iron (Fe^{2+}), methane (CH_4), sulfide (S^{2-}), organic carbon, taste and odor concerns, and naturally occurring hazardous compounds (e.g., arsenic [As]). Fortunately, this 'plume' of impacted groundwater is usually confined within the original contaminant plume and is unlikely to adversely impact potable water supplies.

This report presents the results of research performed as part of project ER-2131 "Numerical Modeling of Post-Remediation Impacts of Anaerobic Bioremediation on Groundwater Quality" supported by the Strategic Environmental Research and Development Program (SERDP) and performed by a team of researchers from North Carolina State University (NCSU) and the United States Geological Survey (USGS).

OBJECTIVES

The overall objective of this research is to develop an improved understanding of the near- and long-term impacts to groundwater quality after implementation of *in situ* anaerobic bioremediation processes. Specific objectives achieved during this project include:

A. Formulate a general modeling approach appropriate for simulating the production and subsequent natural attenuation of SWQIs for a wide range of sites. The model approach and validation was based on data from the Bemidji Crude Oil Spill and Cape Cod Wastewater Plume.

B. Assemble a database of SWQIs at ERB sites to determine the range of SWQI concentrations and evaluate trends over time and distance downgradient.

C. Use the validated modeling approach and results from the database analysis to develop a general conceptual model of SWQI formation, mobilization, and attenuation. This conceptual model can be used to identify sites where SWQI could be an issue and develop monitoring and management approaches to minimize adverse impacts.

TECHNICAL APPROACH

A reactive transport model was developed to simulate the production and natural attenuation of important electron acceptors and SWQI parameters including organic carbon, O_2, NO_3^-, Mn^{2+}, Fe^{2+}, SO_4^{2-}, S^{2-}, CH_4, and CO_2. The behavior of these and other reactive species in groundwater have been intensively studied for many years by the USGS Toxics Substances Hydrology Program (Toxics Program). Model simulation results were compared to an extensive database on monitoring results from two Toxics Program sites: (a) Bemidji Crude Oil Spill, MN; and (b) Cape Cod MMR Wastewater Plume, MA.

SWQI data were collected from 47 active and former ERB sites across the United States, including different contaminants of concern (COCs), injection strategies, organic substrates, and geographic locations. Monitoring data was compiled on SWQI parameters in 917 different monitoring wells from regulatory monitoring reports, DOD (i.e., AFCEE, ESTCP, SERDP) project reports, journal articles, and personal correspondence with site project managers. Summary statistics (mean, median, standard deviation, etc.) and cumulative frequency distribution plots were generated for upgradient, treatment zone, and various downgradient locations to define the range of SWQIs impacts and evaluate trends over time and distance downgradient.

The reactive transport model and SWQI database were then used to produce indicator simulations that illustrate the major processes control the formation and natural attenuation of SWQIs at ERB sites. The model was used to simulate the fate of the added organic carbon and how the reduced products affected the aquifer over a period of 40 years following substrate addition.

Results from the reactive transport model development, SWQI database, and indicator simulations were integrated to develop a general conceptual model of the major processes controlling SWQI production and attenuation. This conceptual model can be used as a guide in understanding the magnitude, areal extent, and duration of SWQIs in ERB treatment zones and the natural attenuation of SWQI parameters as the dissolved solutes migrate downgradient with ambient groundwater flow.

RESULTS

Reactive Transport Model Development

Reactive transport models were created for USGS long-term study sites where reducing conditions were created in shallow aquifers by crude oil (Bemidji) or wastewater disposal (Cape Cod). The goal of the modeling was to understand the creation, natural attenuation, and longevity of the SWQIs created by the reducing conditions. The model simulations described flow and reactions along two-dimensional vertical cross sections of the study aquifers. Steady-state models of the flow systems were created using MODFLOW (Harbaugh, 2005) and reactive transport simulations were performed with PHT3D (Prommer et al., 2003).

For the Bemidji Crude Oil Spill, the goal of the modeling was to understand the generation and fate of the most important SWQIs at the site, especially CH_4, aqueous Fe(II), and dissolved organic carbon (DOC). To constrain the model, complete datasets were assembled for four time points representing the time of the oil spill in 1979 (i.e., immediately after the oil spill), 1987±2 years, 1993±2 years, and 2008±2 years. The model formulation included multiple hydrocarbon compounds in the oil, dissolved hydrocarbons, sediment and aqueous Fe and Mn, mineral controls on pH and alkalinity, and outgassing of CH_4 and carbon dioxide (Ng et al., 2015). The simulation covered the time period from 1979 to 2008 along a 260-m horizontal by 7-m vertical cross-section. Other aspects of the model including initial concentrations, grid discretization, permeabilites, dispersivities, dissolution, equilibrium and kinetic reactions, outgassing, and sorption are described in Ng et al. (2015).

For the Cape Cod Wastewater Plume, the modeling goal was to understand what controlled the recovery rate of aerobic conditions in the aquifer after the cessation of wastewater disposal. The time frame of recovery depended on re-oxidation rates of two pools of reduced species that had accumulated on the aquifer sediments during the 60 years of wastewater disposal pond operations. These two species are sediment-bound biogenic organic carbon located below the disposal ponds and sorbed Fe[II] located in the aquifer downgradient of the ponds. The initial geochemical conditions in the model were based on observations at the time of disposal cessation in 1996. The initial spatial distribution of sediment-bound organic carbon and reaction rates were calibrated to the observed aquifer recovery rates in the first 10 years after cessation. Competitive sorption parameters for major cations, Fe[II], Mn[II], and H^+ were based on laboratory experiments.

SWQI Database

Analysis of the SWQI database results provided significant insights into the production and attenuation of SWQI parameters. Maximum TOC concentrations decline rapidly with distance downgradient of the injection zone. As a result, CH_4 production and SO_4^{2-} reduction are largely restricted to the injection zone and immediately downgradient.

Dissolved Mn and Fe concentrations increased in the injection zone at essentially all sites, then declined with distance downgradient. At >50 m downgradient, the median increase in dissolved Mn and dissolved Fe was 0.08 mg/L and 0.38 mg/L, respectively. Arsenic was not monitored at most sites. When monitoring data was available, arsenic concentrations often increased following ED addition. Increasing dissolved arsenic concentrations were correlated with increasing Fe concentrations consistent with arsenic release during reduction of Fe oxides and/or arsenic removal during sorption/co-precipitation with Fe. In the injection area, sulfate concentrations were often reduced by one to three orders of magnitude, but were not completely depleted at most sites. Further downgradient, the change in sulfate concentration was smaller, indicating substantial attenuation of the low sulfate plume. Sulfide concentrations typically increased by less than 1 mg/L in injection area wells. The maximum increase in CH_4 concentration declines with distance downgradient, indicating some attenuation. However, there were a significant number of wells at greater than 50 m downgradient with high CH_4 levels (>10 mg/L).

While SWQIs were detected in downgradient wells, the large majority of these wells were within the primary contaminant plume. In wells where chlorinated ethenes were previously below maximum contaminant levels (MCLs), SWQIs were generally within background levels or within a few meters of the injection zone. As a result, SWQI production is unlikely to adversely impact potable water supplies.

Indicator Simulations

Results from the indicator simulations provided insights into the major processes controlling the formation and natural attenuation of SWQIs at ERB sites.

Much of the organic carbon added to the aquifer is fermented to CH_4. In coarse-grained sediments near the water table, CH_4 will degas, potentially removing a significant fraction of the added electron equivalents from the saturated zone. In finer grained sediments, gas bubbles can remain trapped within the pores by capillary forces. Once CH_4 production slows, the CH_4 in these trapped bubbles could potentially dissolve back into groundwater and be carried

downgradient with ambient groundwater flow. CH_4 that is not trapped in gas bubbles or released to the vadose zone will migrate downgradient with the ambient groundwater flow. Aerobic methane oxidation is limited by a zone of low O_2 and low CH_4 that separates the anaerobic, methane-rich SWQI plume and the background unimpacted, aerobic groundwater. If AMO occurs using Fe[III] as the TEA, then iron reduction will be the main process limiting the growth of the dissolved CH_4 plume. However if AMO rates are slow, dissolved CH_4 could migrate downgradient with little attenuation beyond dispersive mixing. Once the primary organic substrate (EVO) is exhausted, CH_4 production stops and the CH_4 concentrations will decline.

Shortly after ED addition, SO_4^{2-} concentrations decline in the injection area and a zone of reduced SO_4^{2-} concentrations begins to migrate downgradient. While sulfide is produced by SO_4^{2-} reduction, downgradient migration is limited by reaction with Fe[II] and precipitation as low solubility sulfide minerals.

ED addition results in release of dissolved Fe^{2+} with depletion of Fe[III] in the injection area sediments. However, downgradient migration of the dissolved Fe^{2+} plume is delayed behind the low O_2 plume by sorption to the sediments. Over time, the zone of depleted sediment Fe[III] grows is projected to grow as dissolved CH_4 reduces Fe[III] in the downgradient aquifer. Once the added ED is degraded, the large reservoir of sorbed Fe[II] remains and is not expected to readily desorb. Over time, dissolved Fe^{2+} concentrations decline due to downgradient migration and subsequent sorption to the aquifer material. As clean aerobic groundwater enters from upgradient, Fe[II] desorbs from the sediment, mixes with O_2, and re-precipitates as Fe[III].

Overall, Mn behaves similarly to Fe with Mn[IV] reduced to dissolved Mn^{2+} in the source area, followed by downgradient migration of Mn^{2+}. The total amount of Mn[II] produced is expected to be much lower than Fe[II] due to the smaller amount of Mn[IV] originally present in many aquifer materials. The zone of depleted Mn[IV] is projected to grow more rapidly than the Fe[III] depleted zone because Mn can be reduced under relatively more oxidizing conditions than Fe. Similar to Fe, downgradient migration of dissolved Mn^{2+} is limited by sorption to the sediments and the dissolved Mn^{2+} dissipates once the ED is depleted.

The aquifer downgradient of ERB sites is expected to be quickly depleted of O_2 following ED addition. Reoxygenation of the aquifer is expected to occur very slowly, even once the ED is depleted, due to the large reservoir of sorbed Fe[II] on the sediments that consumes O_2 transported from upgradient.

BENEFITS

This research has improved our understanding of the near- and long-term impacts to groundwater quality after implementation of in situ anaerobic bioremediation approaches. Project results were used to develop a general Conceptual Model and guidance document "Extent and Persistence of Secondary Water Quality Impacts after Enhanced Reductive Bioremediation". This document provides information on the microbiological and geochemical processes controlling production and attenuation of secondary water quality impacts and typical characteristics of secondary water quality impact plumes and can be used by project managers, consultants, and regulators to evaluating the duration, extent, and magnitude of secondary water

quality impacts and to develop monitoring and management approaches to minimize these impacts.

Several results from this study show that natural attenuation of SWQIs can be effective. The first concerns the fate of aqueous Fe[II] mobilized during the active phase of ERB. Modeling of the Bemidji crude oil spill site demonstrated that 91% of mobilized Fe[II] is readsorbed to the sediments in the reducing zone, preventing migration from the treatment zone (Ng et al., 2015). In addition, a field study of the fate of mobilized arsenic at the Bemidji site shows that the arsenic mobilized by natural attenuation of crude oil is re-adsorbed over the same interval as the Fe[II] (Cozzarelli et al., 2015). Production of CH_4 and transport from the treatment zone can also be a concern during ERB. The Bemidji modeling results show that 70% of the produced CH_4 enters the gas phase and is oxidized before reaching the surface. This greatly limits the migration of CH_4 in the groundwater. The recovery time of aerobic conditions in an aquifer following completion of ERB was examined with modeling of the Cape Cod wastewater study site. The results showed that recovery of aerobic conditions can take decades, but dissolved Fe^{2+} does not appear to migrate long distances (Ng et al., in prep.).

1.0   INTRODUCTION

1.1   ENHANCED REDUCTIVE BIOREMEDIATION AND SECONDARY WATER QUALITY IMPACTS

Electron donor (ED) addition can be very effective in stimulating enhanced reductive bioremediation (ERB) of a broad range of contaminants including chloroethenes, chloroethanes, chloromethanes, chlorinated cyclic hydrocarbons, various energetics (e.g., perchlorate, RDX, TNT), and nitrate (AFCEE, NFESC, ESTCP, 2004). Hexavalent chromium (Cr[VI]) and uranium (U[VI]) can be reduced to less mobile and/or less toxic forms (e.g., Cr[III], U[IV]) (Wielinga et al., 2000; Yurovsky et al., 2009). Similarly, reduction of sulfate to sulfide (sulfidogenesis) can be used to precipitate certain heavy metals (e.g., zinc, cadmium, and cobalt) (Vanbroekhoven et al., 2009). However, ED addition can result in the release of a groundwater 'plume' with reduced levels of dissolved oxygen (O_2), nitrate (NO_3^-), and sulfate (SO_4^{2-}), and elevated levels of dissolved manganese (Mn^{2+}), iron (Fe^{2+}), methane (CH_4), organic carbon, and naturally occurring hazardous compounds (e.g., arsenic [As]) (AFCEE, NFESC, ESTCP, 2004; Hering et al., 2009).

There is growing concern about these 'secondary impacts' of ERB. In most cases, the groundwater downgradient from ERB projects is not toxic, but may have impaired taste, odor, and/or aesthetic quality, possibly making it unsuitable as a potable water source. Increasingly, regulators are requiring documentation of the expected or potential impacts prior to issuing required permits. While secondary impacts are monitored at many ERB sites, little of this data has been compiled in a usable form that can be shared with regulators. Fortunately, there is a wealth of information on the natural attenuation of these same parameters at sites where organic rich materials have entered the subsurface (e.g. wastewater, landfill, and hydrocarbon plumes).

For the purposes of this report, we define secondary water quality impacts (SWQIs) as changes in groundwater quality resulting from *in situ* anaerobic bioremediation that have significant adverse impacts on the beneficial use of the groundwater resource. SWQIs may be temporary or long-lived, expected or unexpected, have significant health consequences or only result in a mild change in the palatability of the water supply. SWQIs do not include contaminants produced from destruction of the primary contaminant, but are strictly limited to those constituents produced by or mobilized due to conditions caused by the *in situ* technology.

1.2   TECHNICAL OBJECTIVES

The overall objective of this research is to develop an improved understanding of the near- and long-term impacts to groundwater quality after implementation of *in situ* anaerobic bioremediation processes. Specific objectives achieved during this project include:

A. Formulate a general modeling approach appropriate for simulating the production and subsequent natural attenuation of SWQIs for a wide range of sites. The model approach and validation was based on data from two intensively studied field sites -- Bemidji Crude Oil Spill and Cape Cod Wastewater Plume.

B. Assemble a database of SWQIs at ERB sites to determine the range of SWQI concentrations and evaluate trends over time and distance downgradient.

C. Use the validated modeling approach and results from the database analysis to develop a general conceptual model of SWQI formation, mobilization, and attenuation. This conceptual model can be used to identify sites where SWQI could be an issue and develop monitoring and management approaches to minimize adverse impacts.

1.3   REPORT ORGANIZATION

This technical report describes work completed to date on this project. Section 2 describes model development and evaluation at the Bemidji and Cape Cod sites. Section 3 describes development of the SWQI database and statistical analysis results. Section 4 presents the indicator simulation results. Section 5 integrates the results from Sections 2, 3 and 4 to develop a general conceptual model of SWQI production and attenuation. Research implications and opportunities are presented in Section 6.

2.0 SWQI MODEL DEVELOPMENT

2.1 INTRODUCTION

One of the goals for this project was to formulate a reactive transport model to simulate natural attenuation of the most problematic chemical species driving SWQIs at ERB sites. These species include Fe^{2+}, Mn^{2+}, sulfide (S^{2-}), CH_4, organic carbon, and total dissolved solids. The behavior of these and other reactive species in groundwater have been intensively studied for many years by the USGS Toxics Substances Hydrology Program (Toxics Program). The modeling goals of this task were accomplished using datasets from two Toxics Program sites: (a) Bemidji Crude Oil Spill, MN; and (b) Cape Cod Wastewater Plume, MA. Together these sites provided a comprehensive dataset to constrain model formulations for the suite of reactions controlling the fates of the chemical species listed above.

Data from the three sites together with existing model results were used to address multiple issues concerning appropriate representations of model reactions. First, the important chemical species controlling the reaction behavior of the target species were identified. Probably the most important contribution of this modeling effort is advanced treatment of reactions between aqueous and solid species. Most of the important reactions controlling Fe^{2+}, Mn^{2+} are reactions of this type. During ERB, reduced species are often sequestered on solids in the treatment zone and the downgradient aquifer, such that reduced conditions persist after treatment has ended. A goal of the modeling was to provide a better understanding of the time required for recovery of aerobic conditions after ERB has ended. At Cape Cod, the slow rate of aquifer recovery since sewage disposal ceased provided an extreme end member for recovery rate.

The sections below provide detailed descriptions of the model results from each site.

2.2 THE BEMIDJI CRUDE OIL PLUME

2.2.1 Background and Objectives

Any source of reduced carbon emplaced in the subsurface can create SWQIs, including petroleum hydrocarbons from leaks and spills of crude oil and refined fuels. In 1979, a pipeline rupture resulted in infiltration of ~2,500 barrels of crude oil to a shallow glacial outwash aquifer near Bemidji, Minnesota. The oil is present in three oil bodies at the water table 3-8 meters (m) below the land surface. One of the three oil bodies, known as the "north pool", has been intensively monitored by the USGS for over 30 years. Site research activities include detailed characterization of aquifer microbiology, geochemistry, and mineralogy (Essaid et al., 2011). Important SWQIs at the site result from CH_4 production (Amos et al., 2005), formation of Fe^{2+} and Mn^{2+} (Baedecker et al., 1993), and transport of non-target dissolved organic carbon (DOC) compounds (Thorn and Aiken, 1998).

The objective of the study was to evaluate the biogeochemical processes that control the spatiotemporal evolution of both the primary organic carbon source and SWQIs. The focus at this site was to better understand the mechanisms leading to the formation and natural attenuation of the Fe^{2+}, organic carbon, and CH_4 plumes. Model simulations (Ng et al. 2015) were used to explore different conceptual models of CH_4 generation and outgassing, formation

of sediment-bound reduced iron, and pH buffering postulated by Ng et al. (2014).

2.2.2 Approach

The approach was to create a comprehensive reactive transport model that accounts for oxidation-reduction (redox) reactions driven by organic carbon and equilibrium reactions with aquifer minerals and groundwater. The model accounts for all features identified as important in previous Bemidji models including different classes of organic carbon in the oil source (including benzene, ethybenzene, xylene (BEX); toluene; nonvolatile dissolved organic carbon (NVDOC), and n-alkanes), outgassing of CH_4 and carbon dioxide (CO_2), multiple pH buffering mechanisms, Fe and Mn mineral phases, reactions with carbonates, and representation of sorption of Fe, Mn, and the hydrogen ion (H^+) (Ng et al. 2015). The conceptual model implemented is based on the data compilation and mass balance analyses described in Ng et al. (2014) and illustrated in **Figure 2.1**.
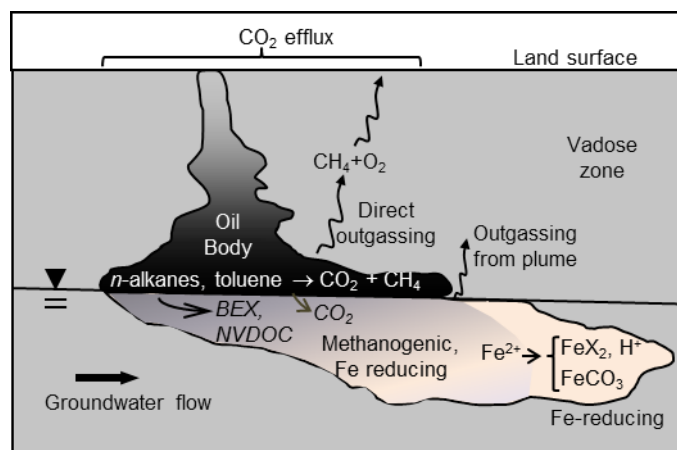
Figure 2.1. Conceptual model of the Bemidji north pool implemented with the reactive transport model. Included are processes not considered in previous Bemidji modeling studies, such as distinct degradation pathways for diverse oil constituents, direct outgassing in addition to outgassing from the aqueous phase, and Fe sorption with H^+ exchange. Taken from Figure (1) in Ng et al. (2015).

Data from 30 years of monitoring were compiled to constrain the model (**Figure 2.2**). New datasets that had not been available in the past were also incorporated, including oil composition, sediment iron extractions, and surface CO_2 efflux. Data representing four time periods were used to constrain the model: (1) the time of the oil spill in 1979; (2) 1987 ± 2 years; (3) 1993 ± 2 years; and (4) 2008 ± 2 years. The data categories include (1) oil characterization and quantification; (2) concentrations of DOC; (3) aqueous concentrations of inorganic groundwater plume constituents; (4) solid iron concentrations from sediment extractions, and (5) surface efflux of CO_2. A detailed list of data sources is provided by Ng et al. (2014) and the data used in the model are available at http://mn.water.usgs.gov/projects/bemidji/data/.

The model PHT3D (Prommer et al., 2003) was used to simulate plume growth for 30 years along a 2-D cross-section of the Bemidji north pool transect. Reactions were implemented using the partial equilibrium (PE) approach (Jakobsen and Postma, 1999) and microbial growth was neglected. In the PE approach, organic carbon oxidation is the rate-limiting step and reduction

of other constiutents is represented as equilibrium reactions. For example, for one mole of benzene (C_6H_6) degrading at a specified rate, six moles of C(-1) and six moles of H(+1) are newly introduced into the equilibrium solution (oxidation states in parentheses). C(-1) then automatically converts to the inorganic carbon form via the Terminal Electron Accepting Process (TEAP) with the most favorable equilibrium thermodynamic conditions in the solution. The equilibrium redox couples needed to simulate the secondary plumes at Bemidji are H^+/H_2, O_2/H_2O, Fe[III]/Fe[II], Mn[IV]/Mn[II], and CO_2/CH_4. Other aqueous phase equilibrium reactions considered include those found in the PHT3D database, such as full carbonate and hydroxide chemistry and re-oxidation. Tables listing the oil components, mineral reactions, initial and boundary conditions, and reaction parameters are provided in Ng et al. (2015).
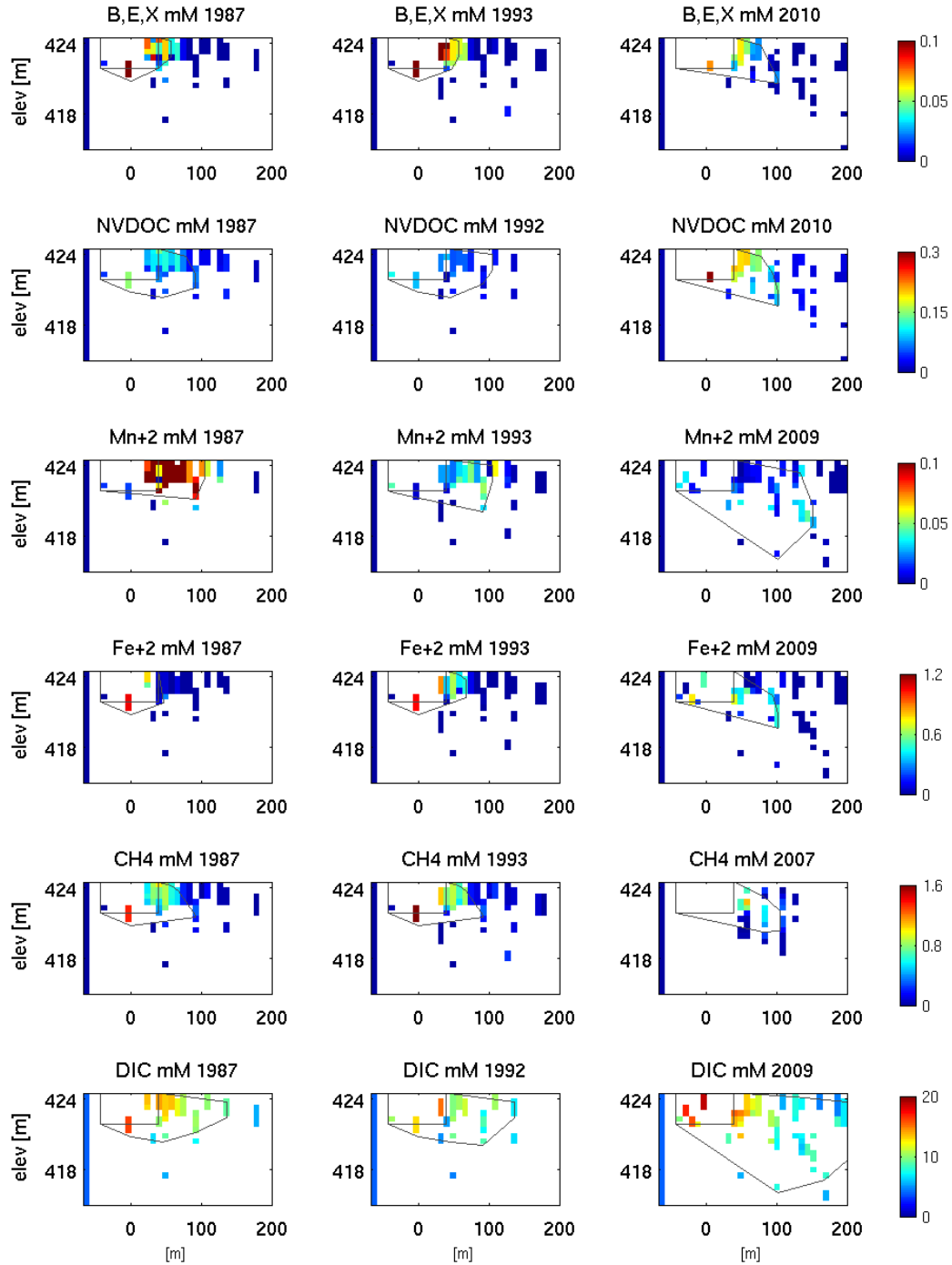
Figure 2.2. Observations of the six major redox species at the three observational periods. Plots include well data from the available year closest to the target year (within ±2 years) and are adapted to our model resolution. Left-hand stripes indicate the background and initial concentrations, determined from upgradient well observations. The boxes correspond to the oil body reference rectangle. The polygons outline the plume extent for the corresponding component, which are delineated around wells with measurements significantly different than background. Adapted from Figures (5) and (6) from Ng et al. [2014].

6

2.2.3   Major Findings

The model results for the major redox species are shown in **Figure 2.3**. The model results capture important features of the plume. These include the limited size of the BEX plume, the growth of the NVDOC plume, the production and subsequent sorption of the Fe[II] and Mn[II] plumes, the production and attenuation of dissolved CH_4, and finally the production and growth of the dissolved inorganic carbon (DIC) plume. The most important findings of the modeling study are summarized below and described in detail by Ng et al. (2015).

The first major finding of the modeling study concerns the fate of the reduced Fe produced by dissimilatory iron-reduction. The Bemidji results show that 99% of the total reduced Fe is in the solid phase on the surface of the aquifer sediments. Immobilization on sediments strongly limits the SWQI from reduced Fe at this site. The model results suggest that the immobilization mechanism is sorption. The role of sorption in sequestration of reduced Fe appears much greater than previously recognized at this and other sites. The model also showed that precipitated siderite serves as an additional Fe sink after existing Fe sorption sites are exhausted. This additional reduced Fe sink can facilitate continued and gradual depletion of ferric oxide minerals. The form of reduced Fe on sediments may affect its stability, which controls the likelihood of remobilization and future plume persistence.

The second major finding concerns the production and fate of CH_4. Most of the CH_4 is produced by degradation of the *n*-alkane fraction of the oil (Ng et al., 2014). The produced CH_4 and CO_2 migrate away from the oil in both the gas- and aqueous-phases (Amos et al., 2005). Depleted nitrogen (N_2) concentrations in wells downgradient from the oil body indicate some outgassing of dissolved CH_4 has occurred (Amos et al., 2005), but dissolved N_2 is not completely depleted, providing a constraint on the CH_4 cycled through the aqueous phase. The model results predict that 86% of observed surface efflux consists of outgassed carbon that could not have cycled through the aqueous phase sampled in the monitoring wells. Direct outgassing is the largest sink for carbon from the source zone, with an estimated 70% of carbon lost by this pathway. Outgassing from the aqueous phase is mostly in the form of CH_4, which is consistent with its much lower solubility compared to CO_2. Preferential outgassing of dissolved CH_4 maintains low CH_4 to CO_2 aqueous concentration ratios, even when the plume is strongly methanogenic.

Two important attenuation mechanisms limit the migration of the produced CH_4. The gas-phase CH_4 that diffuses upward through the vadose zone is oxidized to CO_2 before reaching land surface. The primary natural attenuation mechanism for aqueous-phase CH_4 in groundwater at the Bemidji site appears to be anaerobic methane oxidation (AMO) coupled to Fe reduction (Amos et al., 2012). The existence of AMO coupled to iron reduction has yet to be fully established by identification of the responsible microorganisms. Nevertheless, field evidence at Bemidji (Amos et al., 2012) and other sites indicate that AMO coupled to Fe reduction may play an important role in limiting the SWQIs of CH_4 produced in ERB source zones at some sites.
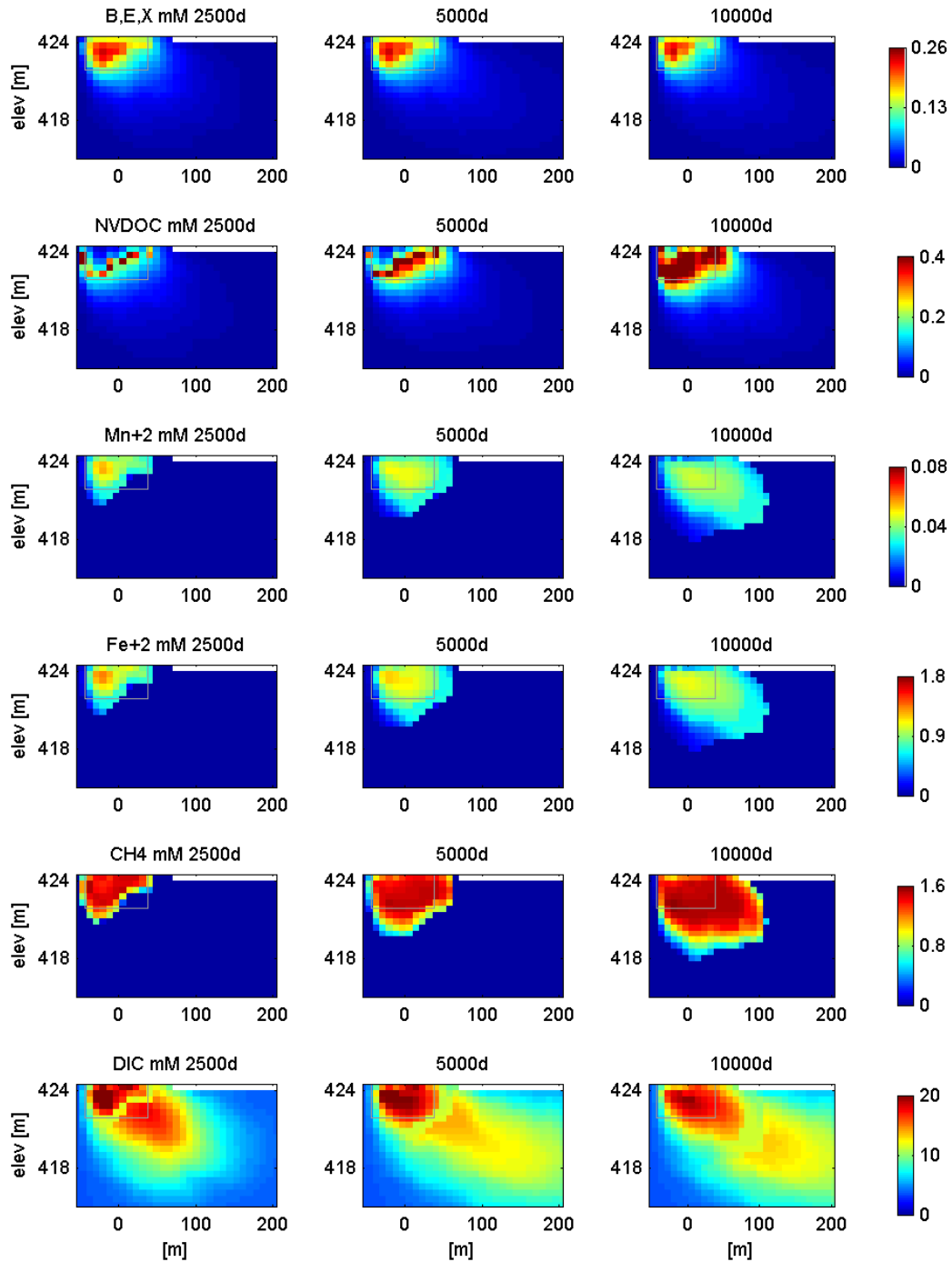
Figure 2.3. Model simulation results for six major redox species at three times corresponding to the observational time periods chosen for the data compilation. Gray boxes correspond to the oil body reference rectangle. BEX and NVDOC represent electron donors. Mn^{2+}, Fe^{2+}, and CH_4 are reduced aqueous species resulting from different anaerobic TEAPs. DIC is produced by all TEAPs.

2.2.4 Important Implications

The Bemidji model results suggest that sorption is the dominant immobilization mechanism. Further studies of this mechanism described in the Cape Cod section explore the role of sorbed Fe[II] as aerobic conditions are re-established in an aquifer.

Methane production occurs primarily in the source zone where low solubility oil components degrade without entering the groundwater plume. The CH_4 is produced in sufficiently large quantities that it enters the gas phase and diffuses toward the surface. Production of CH_4 in the source zone is likely to occur when excess carbon is emplaced at ERB sites. The risk of upward migration of CH_4 toward the land surface depends on the nature and depth of the emplaced carbon.

The database survey shows that dissolved CH_4 plumes extend more than 50 m downgradient of the injection zone at some ERB sites, while at other sites the CH_4 plume appears to be more limited. The Bemidji results provide evidence that AMO coupled to Fe reduction may be an important natural attenuation mechanism for dissolved CH_4 plumes at some ERB sites. Additional research is needed on this process and its reliability at other sites.

2.3   THE CAPE COD WASTEWATER PLUME

2.3.1 Background and Objectives

Almost two decades of groundwater chemistry observations in a wastewater contaminant plume following removal of the source have led to new insights into aquifer recovery following source-cessation. The contaminant plume resulted from nearly 60 years of land-disposal of treated wastewater on western Cape Cod, Massachusetts, USA. The plume affects an unconfined aquifer with glacial outwash sediments comprised of coarse sand and gravel. High sediment permeability combined with a humid climate result in groundwater velocities of approximately 0.4 meters per day (m/d) and rapid plume growth to a length of over 7000 meters in the direction of groundwater flow. The aquifer sediments support poor soils and have very low concentrations of organic carbon. As a result of low loads of organic carbon to the aquifer, uncontaminated groundwater remains oxic with only a small loss of dissolved oxygen over several kilometer-long transport distances. In contrast, during active wastewater disposal the core of the wastewater plume became anaerobic at the source. Monitoring of the plume within 600 meters of the abandoned disposal beds since source-cessation has shown that unreactive wastewater constituents (e.g., boron [B]) were flushed from the study area within 10 years but the core of the plume has remained anoxic with a zone dominated by iron(II) (Fe[II]) (**Figure 4.4**). The accumulation of Fe[II] was the result of anaerobic, microbial reduction of Fe[III] oxyhydroxides associated with sediments, which is driven by inputs of wastewater-derived organic carbon to the aquifer.
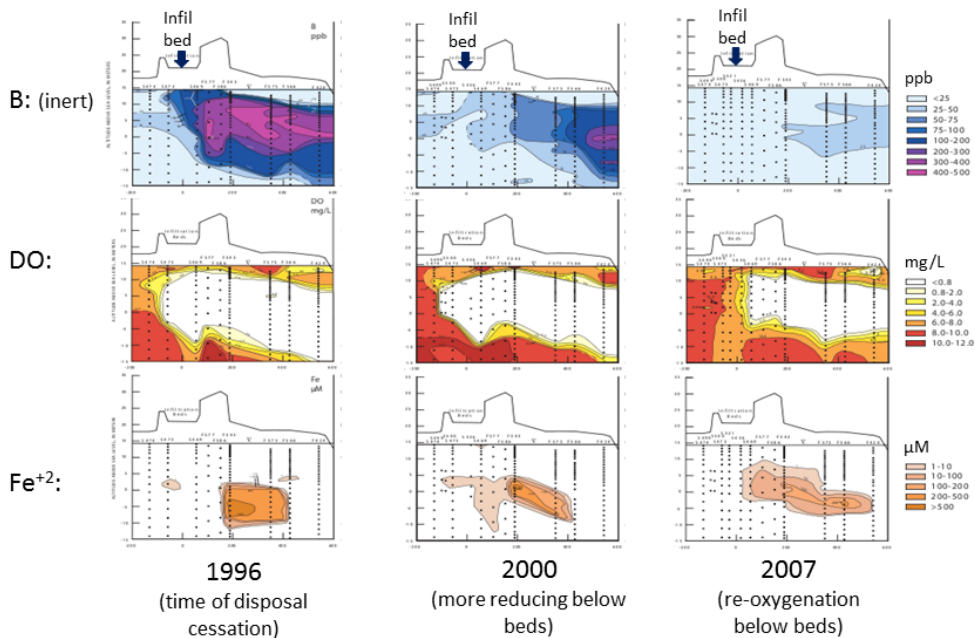
Figure 2.4. Spatial distribution of dissolved constituents over time. Dissolved boron (top), oxygen (middle) and Fe(II) along a two-dimensional cross section through the wastewater plume near the time of source cessation (left column), four years after source cessation (center column), and 11 years after source cessation (right column).

The modeling objectives of plume evolution at the Cape Cod site are three-fold. First, we want to develop a transferable modeling approach to simulate redox evolution driven by microbial metabolic processes. Second, we want to illustrate the importance of accounting for sorption of Fe[II], how Fe[II] sorption is coupled to sorption of other solutes, and how these sorption reactions are coupled to microbial redox reactions. Third, we want to understand the processes controlling re-oxygenation of the anaerobic plume following source-cessation.

2.3.2   Approach

In order to achieve the modeling objectives, we first developed a reactive transport model that simulated the changes in O_2, Fe[II], pH, and other constituents observed over the nearly 10 years since source-cessation. We then applied this model to predict the evolution of redox conditions in the plume until the aquifer became fully oxygenated within the spatial domain of the model. The microbial metabolism during recovery is fueled by the labile fraction of organic carbon on the aquifer sediments. The source of this labile organic carbon appears to be mainly from microbial growth and microbial polymers formed during the period of active wastewater disposal into the aquifer. We hypothesize that this labile organic carbon, which will be called biogenic, mixed-stoichiometry organic carbon (BMSOC), is a very small fraction of the total organic carbon on the sediment and may not correlate with organic carbon quantified using typical assays. We used the model to examine the role of BMSOC and sediment-bound Fe[II] in

10

limiting the advancement of O_2 through the plume and examined the sensitivity of the simulated evolution of plume chemistry to key parameters in the model.

The model was constructed along a two-dimensional vertical transect through the aquifer. A two-dimensional, steady, groundwater flow field was set up to resemble the average flow field observed in the study area and to match the slope along the direction of flow of the vertical boundary between the anoxic plume and oxic, uncontaminated zone above it. The observed biogeochemical zones in the plume prior to source cessation were established within the spatial domain of the model and include: oxic, anoxic with nitrate, and anoxic with Fe[II] and manganese (Mn[III/II]) (**Figure 2.5**). A set of chemical reactions was included to describe competitive sorption among the major cations (Na^+, K^+, Mg^{2+}, Ca^{2+}), Fe[II] and Mn[III/II], and H^+. Parameters in the sorption model were calibrated using laboratory experiments with site-specific sediments (Kohler and Kent, in prep.). The initial spatial distribution of BMSOC and the rates of aerobic respiration and anaerobic respiration (coupled to NO_3^- or Fe[III] reduction) were calibrated using 1) the observed slow advance of the front of O_2 beneath the abandoned wastewater disposal beds; 2) the observed evolution of redox conditions within the plume downgradient of the source following source cessation; and 3) the evolution of pH in the anaerobic plume following source cessation.
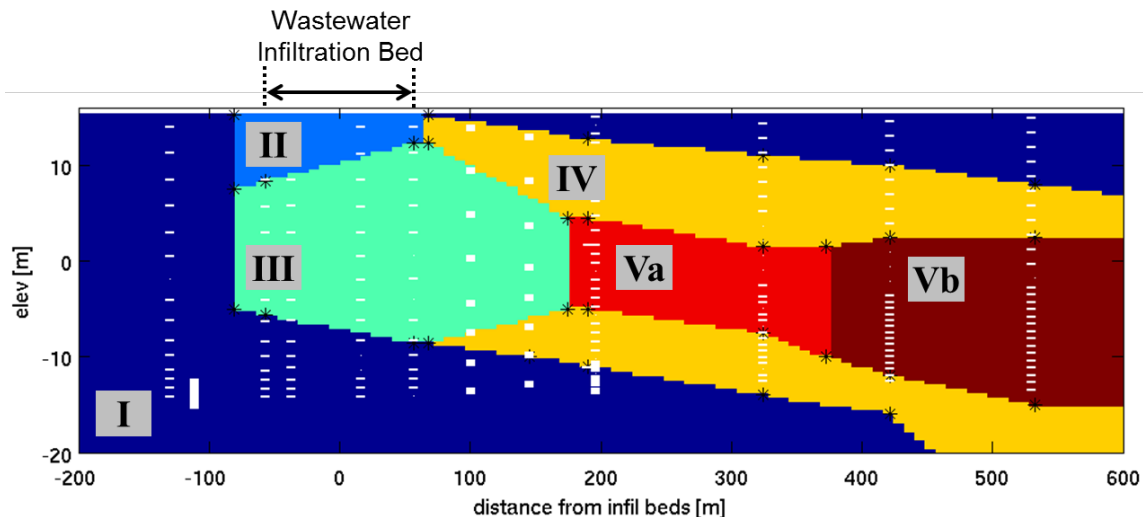
Figure 2.5. Groundwater flow field (arrows) and geochemical zones in groundwater model. Biogeochemical zones: I (oxic, uncontaminated); II (oxic, contaminated, directly under disposal beds; III (anoxic with nitrate, under disposal beds and immediately downgradient); IV (anoxic with nitrate); and anoxic with Fe[II] (Va) or Mn (Vb) along the two-dimensional vertical cross section model domain.

2.3.3 Major Findings

Simulations show that the O_2 front advances much more slowly than the groundwater velocity (Ng et al., in prep.), as was observed in the field (**Figure 2.4**). Unreactive constituents were transported out of the model domain in a few years but the model predicts that re-oxygenation

will require a few decades. Simulation results show that both BMSOC and sorbed Fe[II] control the time required for re-oxygenation.

Simulation results show that BMSOC is an important control on the rate of re-oxygenation of the wastewater plume, especially in the regions under the abandoned wastewater disposal beds and between the abandoned disposal beds and the Fe[II] zone (zone III in **Figure 2.5**) (Ng et al., in prep.). The distribution of BMSOC in the model is shown in **Figure 2.6**. The maximum BMSOC sediment concentration, which occurs under the abandoned wastewater disposal beds, is 0.6 micromoles C per gram of sediment (µmol/g) (Ng et al., in prep.). For comparison, total and water-extractable organic carbon concentrations observed on sediments under the disposal beds were 20-50 and 9-30 µmol/g, respectively (Smith et al., 2013). Previous calculations showed that a value of 0.7 µmol/g for metabolizable organic carbon on the sediment could account for the observed rate of travel of O_2 under the abandoned disposal beds (Smith et al., 2013). Thus, the concentration of sediment-bound organic carbon that drives microbial respiration in the wastewater plume is very low and does not correspond to any form of sediment-bound organic carbon thus far measured. The model-calibrated first-order rate of oxygen consumption coupled to BMSOC degradation (Ng et al., in prep.) is also considerably lower than oxygen consumption rates measured in batch incubations reported in Smith et al. (2013).
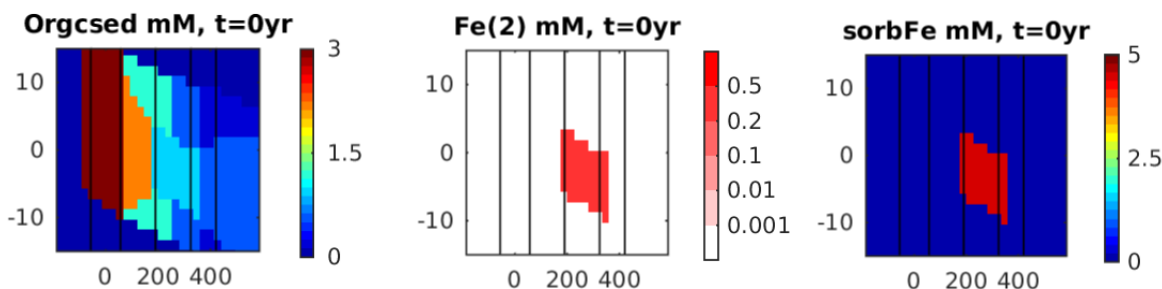
Figure 2.6. Initial spatial distribution of concentrations of reactive organic carbon (top), dissolved Fe[II] (middle), and sorbed Fe[II] (bottom) used in simulations.

In addition to BMSOC, sorbed Fe[II] plays an important role in delaying re-oxygenation of the anoxic zone of the wastewater plume (Ng et al., in prep.) (**Figure 2.7**). Sorbed Fe[II] owes its existence to wastewater derived organic carbon, which drove dissimilatory Fe[III] reduction in the anoxic core of the plume. Observed growth of the Fe[II] zone after cessation of wastewater disposal (**Figure 2.4**), driven by anaerobic microbial metabolism, was used to calibrate the initial concentration of BMSOC in the region downgradient from the abandoned disposal beds and to constrain the rate constant for anaerobic biodegradation. The relationship between dissolved and sorbed Fe[II] concentrations is described by the sorption model and controlled by pH and the major cation concentrations. The model-predicted concentrations of sorbed Fe[II] in the Fe[II] zone at the time of source cessation is in good agreement with extractions of Fe[II] from sediments collected from that zone. Sorbed Fe[II] concentrations exceed dissolved concentrations by a factor of 20 or more, depending on local chemical conditions.
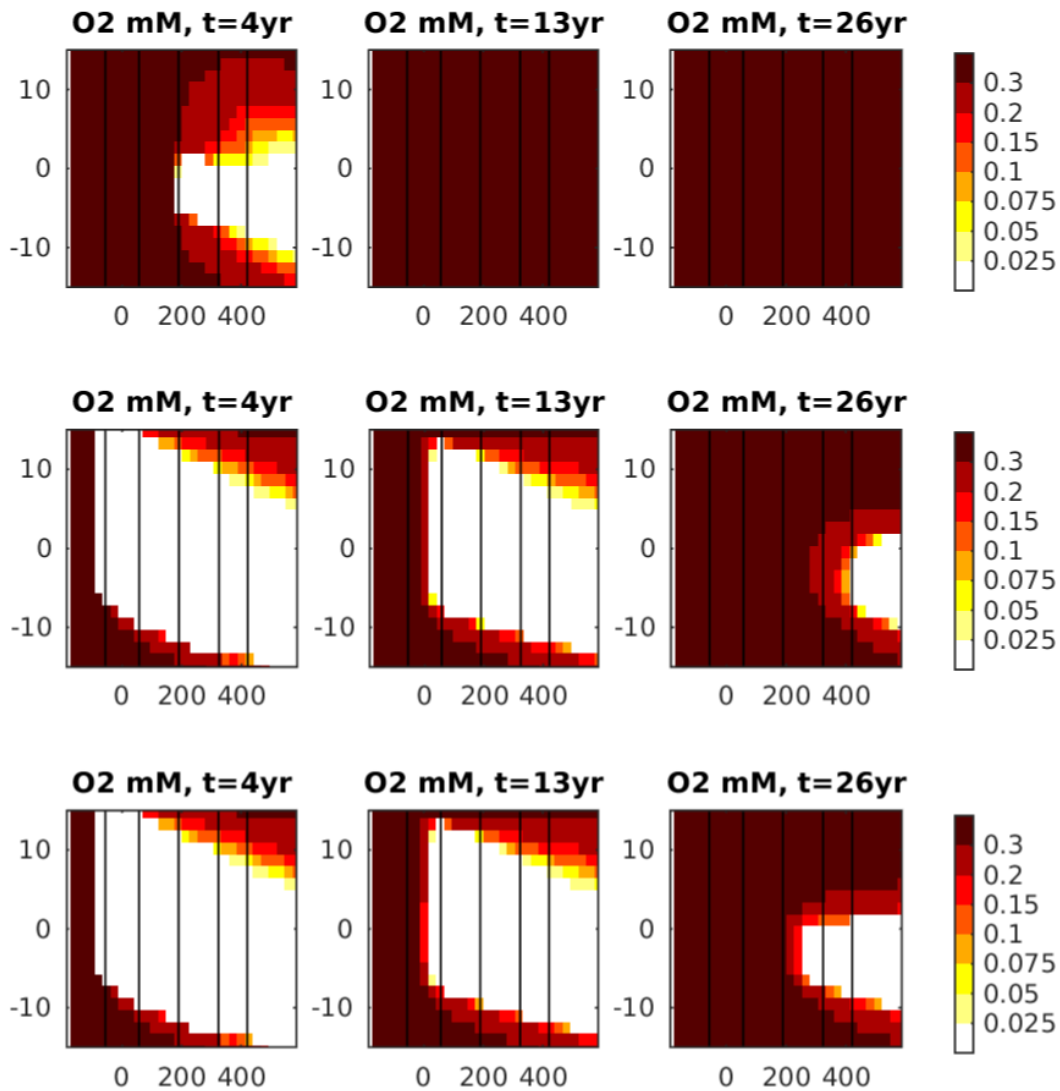
Figure 2.7. Simulated spatial distributions of dissolved oxygen 4years after source-cessation (left-hand column), 13 years after source-cessation (center column), and 26 years after source-cessation (right-hand column) based on three different scenarios. Top row: oxygen removal by oxidation of dissolved and sorbed Fe[II] but no removal coupled to microbial oxidation of organic carbon. Middle row: oxygen removal by microbial oxidation of organic carbon and dissolved Fe[II] but no sorbed Fe[II]. Bottom row: oxygen removal by microbial oxidation of organic carbon and oxidation of dissolved and sorbed Fe[II].

The role of aerobic respiration coupled to BMSOC and oxidation of sorbed Fe[II] in controlling the rate of re-oxygenation of the wastewater plume is compared in **Figure 2.7**. In the absence of aerobic respiration coupled to BMSOC, the dissolved oxygen front advances rapidly to the region with elevated sorbed Fe[II] (**Figure 2.7**, top row, left panel). Oxidation of the sorbed

13

Fe[II] is complete sometime prior to 13 years after source cessation, at which point the former wastewater plume is predicted to be fully oxic (**Figure 2.7**, top row, middle panel). In the absence of sorbed Fe[II] but presence of dissolved Fe[II] at concentrations observed at the time of source-cessation (**Figure 2.4**), the dissolved oxygen front moves slowly through the aquifer as observed (**Figure 2.7**, center row). However, simulated pH values in the downgradient region with elevated dissolved Fe[II] concentrations increase to the point where the Fe[II] carbonate mineral siderite precipitates (Ng et al., in prep.). Precipitation of siderite in the model is inconsistent with field observations showing that siderite has remained undersaturated by a factor of 10 or more in the wastewater plume. The O_2 front moves slowly once it encounters the region with siderite (**Figure 2.7**, center row, right-hand panel). In the full simulation (**Figure 2.7**, bottom row), the O_2 front moves slowly directly under the abandoned wastewater disposal beds, more rapidly in the region between the disposal beds and the region with elevated dissolved and sorbed Fe[II], then slowly through the region with sorbed Fe[II].

H^+ is a reactant or product in both redox (e.g., Abrams et al., 1996; Hunter et al., 1998; Bethke et al., 2011) and sorption reactions (Davis et al., 1998; Kent et al., 2007). Therefore, spatial and temporal distributions of pH can provide important constraints for models incorporating biodegradation. This is especially true where dissimilatory Fe[III] reduction is important because it drives pH up (e.g., Abrams et al., 1996). In our model, if the rate of anaerobic biodegradation is too high, simulated pH values greatly exceed those observed in the field (Ng et al., in prep.). Conversely, if the rate of anaerobic biodegradation is too low, dissolved Fe[II] concentrations are unrealistically low. Concentrations of Fe[II] and pH values also constrain the concentration of BMSOC downgradient of the abandoned wastewater disposal beds. Sorption reactions also influence Fe[II] concentrations and pH values but parameters describing these reactions are constrained by laboratory experimental data (Kohler and Kent, in prep.). Perturbations in sorption parameters required to mitigate excessive pH values or insufficient Fe[II] concentrations in the model fall outside of the range consistent with the results of laboratory experiments.

2.3.4 Important Implications

Addition of the organic carbon source in ERB will promote microbial growth, which will subsequently result in the accumulation of biogenic organic carbon on sediments near the source. This biogenic organic carbon may drive microbial metabolism long after depletion of the injected carbon source, contributing to the persistence of anaerobic conditions in the aquifer near and downgradient from the source after treatment ends.

Addition of organic carbon will stimulate production of Fe[II] through dissimilatory Fe[III] reduction. The extent to which sorbed Fe[II] accumulates on sediments will depend on local chemical conditions, namely pH and major cation concentrations. Elevated pH values and low dissolved salt concentrations favor increased sorption and, therefore higher concentrations of sorbed Fe[II]. Fe[II]-containing secondary phases, such as siderite, green rust, or magnetite, could form as well, but nucleation and growth of these phases can be limited. Sorbed Fe[II] will be an important component of the Fe[II] pool that retards the re-oxygenation of aquifers following ERB treatments.

Iron(II) sorption is influenced by pH, which, in turn, is controlled by redox and sorption reactions. Reduction of Fe[III] oxyhydroxides to Fe[II] has an especially large impact on pH

because three moles of hydroxide (OH$^-$) are released per mole of Fe[III] reduced. Both products of Fe[III] reduction (OH$^-$ and Fe[II]) participate in sorption reactions that also involve major cations and other groundwater constituents. Accounting for the evolution of pH in predictive simulations requires proper description of both redox and sorption reactions. Because of this, observations of pH can provide insight into important process occurring in the sub-surface and can help constrain models for predicting secondary water quality impacts of ERB.

3.0   SWQI DATABASE

3.1   INTRODUCTION

While ED addition will drive the biotic and abiotic destruction and/or immobilization of a broad range of groundwater contmainants, it often results in the production of SWQIs at ERB sites. These SWQIs could potentially have adverse impacts on the beneficial use of the groundwater resource. SWQIs may be temporary or long-lived, expected or unexpected, have significant health consequences or only result in a mild change in the palatability of the water supply. For this article, SWQIs do not include degradation products produced from the primary contaminant, but are limited to those constituents produced by or mobilized due to conditions caused by ERB.

The most common approach for stimulating ERB involves addition of a fermentable organic substrate to the aquifer to serve as an electron donor and carbon source for microbial growth. The choice of substrate and the method of injection depend on the contaminant type and distribution in the aquifer, hydrogeology, and remediation objectives. Organic substrate can be added using conventional well installations, by direct-push technology, or by excavation and backfill. Injection points may be arranged in a grid to treat source areas or in a line perpendicular to groundwater flow to form a PRB. Slow-release products composed of edible oils or solid substrates tend to stay in place for an extended treatment period. Soluble substrates or soluble fermentation products of slow-release substrates can potentially migrate into and disperse within heterogeneous lithologies via advection and diffusion, providing broader but shorter-lived treatment zones. The added organic substrates are first fermented to hydrogen (H_2) and volatile fatty acids (VFAs). The VFAs, including acetate, lactate, propionate, and butyrate, provide carbon and energy for bacterial metabolism.

At a few sites, concerns have been raised regarding the formation and mobilization of SWQIs following ERB. USEPA (2009) has established secondary maximum contaminant levels (MCLs) for a number of SWQIs including Fe, Mn, and total dissolved solids. Hering et al. (2009) and He et al. (2010) showed that arsenic could be temporarily mobilized during ERB of chlorinated solvents at Fort Devens, Massachusetts. At the Grants Chlorinated Solvent Plume Superfund Site, a vapor intrusion program was implemented to determine if there was potential for methane and hydrogen sulfide accumulation (USEPA 2013).

To gain a better understanding of the formation and extent of SWQIs at ERB sites, monitoring data from 47 active and former ERB sites was compiled and analyzed to determine the range of SWQIs and evaluate trends over time and distance downgradient. This information was then used to develop a general conceptual model of SWQI production in treatment zones and attenuation during downgradient transport.

3.2   DATABASE DEVELOPMENT

SWQI data were collected from 47 ERB sites across the United States. These sites are illustrative of the wide range of conditions found at ERB field sites, including different contaminants of concern (COCs), injection strategy, organic substrates, and geographic location. Data was collected from regulatory monitoring reports, DOD (i.e., AFCEE, ESTCP, SERDP) project reports, journal articles, and personal correspondence with site project managers. A list of the sites included in the database, including site name, location, injection type, organic substrate, data source, and length of data record, is provided in **Table A-1** in **Appendix A**.

Once site reports containing pre- and post-injection SWQI data were collected, the data were tabulated for statistical analysis. Data collected from each site included: concentrations of COCs and daughter products, SWQIs, and terminal electron acceptors (TEAs); field parameter values (e.g., pH, specific conductance, turbidity); injection data (injection strategy, amount and type of ED, addition of other amendments); and hydrogeologic information (groundwater velocity, hydraulic conductivity, lithology). Concentrations reported as below detection were entered into the database at half the detection limit, with a note stating the parameter was not detected. Summary statistics (mean, median, standard deviation, etc.) and cumulative frequency distribution plots were generated for upgradient, treatment zone, and various downgradient locations.

3.3   REMEDIATION SYSTEM CHARACTERISTICS

The ERB projects included in our survey used a variety of different organic substrates including soluble substrates (14 sites), low solubility liquid substrates (21 sites), solid substrates (2 sites), and mixed or multiple substrates (10 sites). The injected substrates were introduced into the subsurface as source area point injections (32 times), PRBs (16 times), recirculation systems (7 times), biowalls (mulch or mulch and soybean oil) (4 times), or horizontal wells (1 time). The sum of these is greater than 47 because some sites received multiple injections as different injection types.

In addition to the primary substrates, some ERB sites were also amended with pH buffering reagents (e.g., bicarbonate, carbonate) (10 sites); bioaugmentation cultures (e.g., KB-1$^{®}$, SDC-9) (9 sites); *in situ* chemical reduction reagents (e.g., ferrous sulfate, gypsum) (5 sites); and nutrients to aid biological growth (e.g., diammonium phosphate, yeast extract, vitamin B_{12}) (5 sites). Available monitoring data ranged from 4 months to 11 years post-injection. When additional iron (5 sites) or sulfate (2 sites) was added as part of the remediation process, data on iron and/or sulfate concentrations from these sites were not included in the general statistical analysis.

Table 3.1 shows the range of remediation site characteristics including number of monitoring wells, monitoring duration, estimated groundwater velocity at the site, vertical injection interval, width of barrier or area treatment perpendicular to flow, length of treatment zone parallel to flow, and amount of carbon added. Estimated groundwater velocity varied greatly from 2 to 350 meters per year (m/yr). Many of the remediation systems were relatively small and served as pilot systems to evaluate system performance before moving to full-scale remediation. The median length of the injection zone parallel to flow was small since many of the remediation systems were designed to operate as PRBs to limit contaminant migration.

Table 3.1. Treatment System Characteristics in Survey Population.

Parameter	Units	n	Percentiles						
			Min.	10th	25th	50th	75th	90th	Max.
Monitoring wells per site	wells	47	2	6	9	14	24	40	136
Monitoring Duration	yr	47	4	7	12	22	50	77	132
GW Velocity	m/yr	36	0.8	3	5	35	94	250	350
Travel time to most downgradient well	yr	36	0.03	0.06	0.2	0.6	2.7	18	48
Vertical Treatment Interval	m	33	2	3	3	6	6	9	20
Monitoring Period Post-Injection	yr	47	0.3	0.6	1.0	1.8	4.1	6.4	11
Monitoring Period/ Travel time	yr/yr	36	0.02	0.1	0.5	2.5	10	17	43
Treatment Width Perpendicular to GW Flow	m	33	1	4	9	14	30	67	390
Treatment Length Parrallel to GW Flow	m	33	0.5	1	3	3	9	15	76
Carbon Injected	Tonne	33	0.03	0.12	0.33	1.1	2.7	11	70
Injection Barrier Carbon	kg/m^2	13	2	5	7	19	30	61	129
Mulch Biowall Carbon	kg/m^3	2	19	19	20	21	21	22	22
Area Treatment Carbon	kg/m^3	18	0.2	0.4	1	3	8	33	72

3.4   SWQI PARAMETER CUMULATIVE FREQUENCY DISTRIBUTIONS

Table A-2 in Appendix A provides summary statistics for post-injection monitoring data for all upgradient, injection area, and downgradient wells at the 47 sites contained in the database. Downgradient wells include monitoring points outside of the target treatment zone and up to 760 m downgradient. **Figure 3.1** shows cummulative frequency distributions for most of the tablulated SWQI parameters in monitoring wells located upgradient, within the injection area, and at varying distances downgradient. USEPA MCLs are shown for reference where applicable (USEPA 2009). For parameters that generally increase following ERB (total organic carbon [TOC], Fe, Mn, As, S^{2-}, CH_4), maximum values are shown, while minimum values are shown for parameters that generally decrease (oxidation-reduction potential [ORP], SO_4^{2-}). Maximum or minimum values are reported because average values may be biased by measurements collected before the organic substrate reached the well or after it was depleted. For parameters that may increase or decrease (pH), median values are shown. **Figure 3.2** shows cumulative frequency distributions for the change in measured values for these same parameters. Values plotted are delta (Δ) concentration maximum or minimum value (C) minus pre-injection value (C_o) or C/C_o, depending on which approach best illustrated the results.
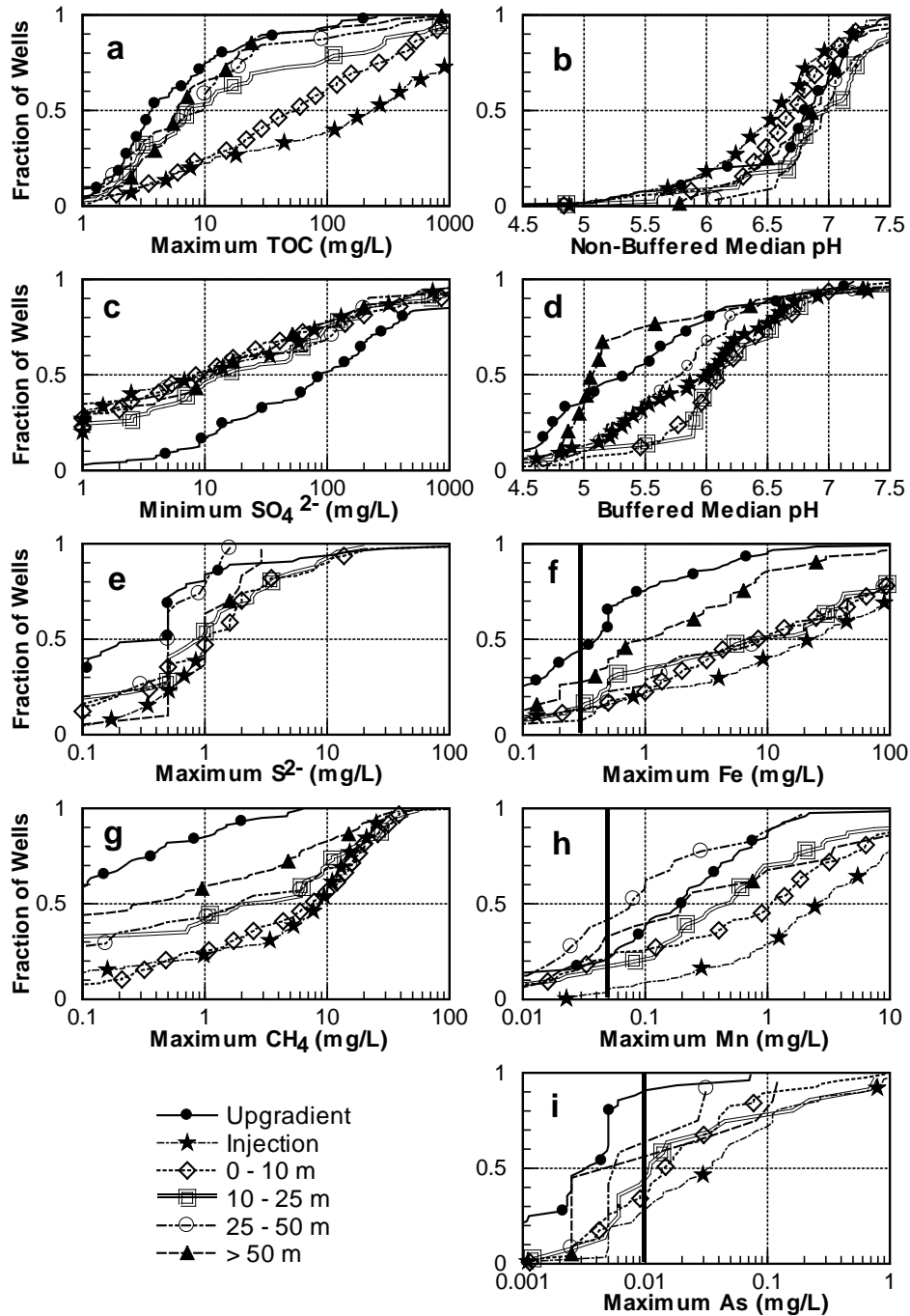
Figure 3.1. Cumulative frequency distributions for SWQI concentrations at 47 ERB sites.
Figures show measured values of upgradient, injection area, and downgradient monitoring wells
for: a) maximum total organic carbon (TOC); b) median pH for non-buffered sites; c) minimum
dissolved sulfate (SO_4^{2-}); d) median pH buffered sites; e) maximum dissolved sulfide (S^{2-}); f)
maximum dissolved iron (Fe); g) maximum dissolved methane (CH_4); h) maximum dissolved
manganese (Mn); and i) maximum dissolved arsenic (As). MCL is shown by black vertical line.
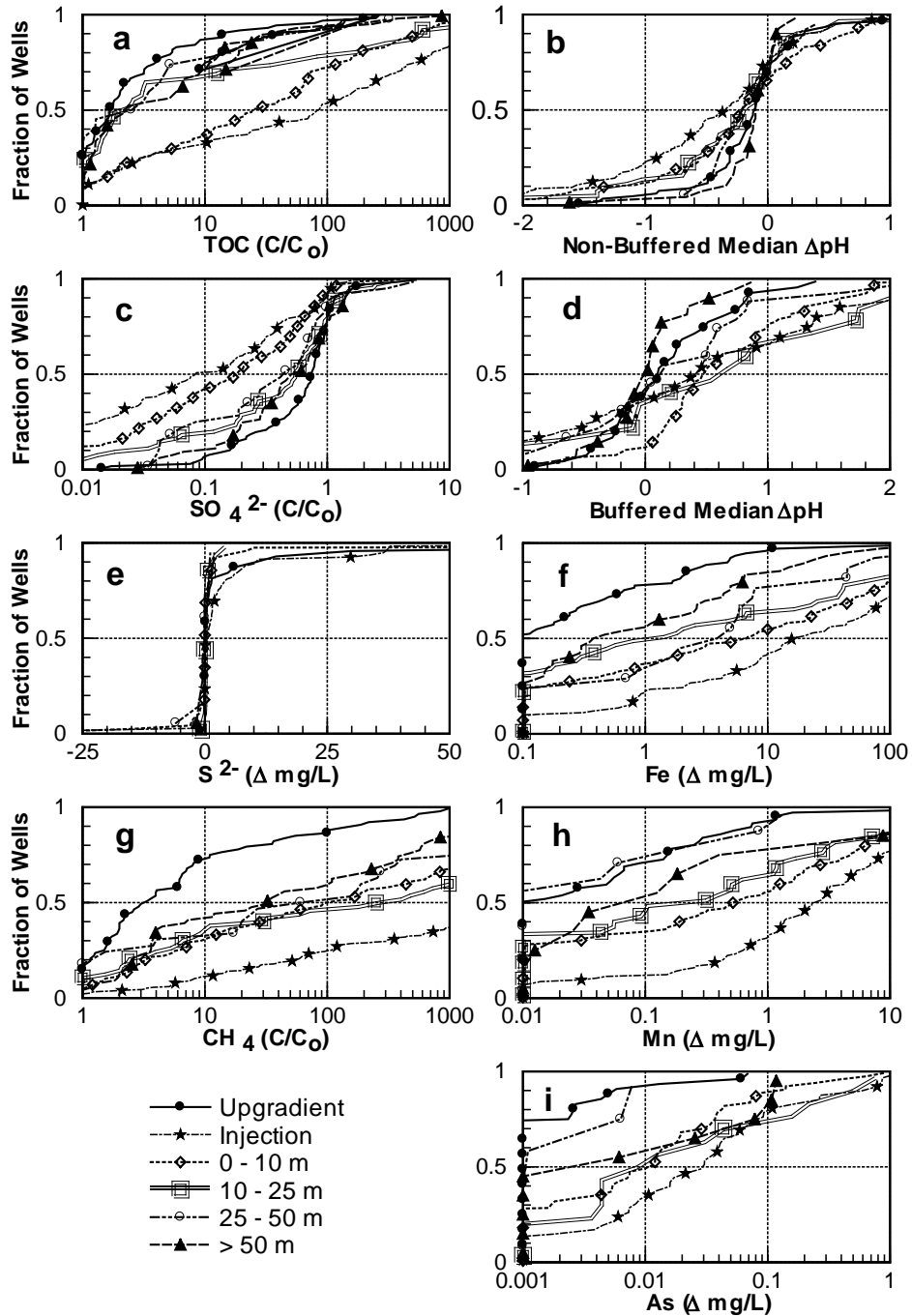
Figure 3.2. Cumulative frequency distributions for change in SWQI concentrations at 47 ERB sites. Figures show change in measured values in upgradient, injection area, and downgradient monitoring wells: a) total organic carbon (TOC); b) pH for non-buffered sites; c) dissolved sulfate (SO_4^{2-}); d) pH for buffered sites; e) dissolved sulfide (S^{2-}); f) dissolved iron (Fe); g) dissolved methane (CH_4); h) dissolved manganese (Mn); and i) dissolved arsenic (As). Δ indicates maximum observed value minus pre-injection value at that well. C/C_o indicates maximum (or minimum) observed value divided by pre-injection value at that well. For pH, change is difference between median post-injection and pre-injection value at the well.

Maximum observed TOC concentrations and changes in concentrations are shown in **Figures 3.1a** and **3.2a**. As expected following organic substrate addition, injection area concentrations were substantially elevated compared to upgradient concentrations. For instance, the median injection area TOC concentration is nearly two orders of magnitude higher than the median upgradient TOC concentration. However, TOC concentrations decline rapidly with distance, dropping almost an order of magnitude in the 0-10 m wells. At greater than 10 m downgradient, the median TOC was 2- 2.5 times the pre-injection value.

Figure 3.1b and **3.1d** shows median post-injection pH values for wells at sites with and without buffer addition. The ΔpH values shown in **Figures 3.2b** and **3.2d** are the difference between the median pH and the value prior to injection. At non-buffered sites, the background pH is slightly below neutral (**Figure 3.1b**). The largest pH declines occur in wells closest to the injection area and lessen with distance downgradient (**Figure 3.2b**). The range of ΔpH values for wells 0-10, 10-25, 25-50, and >50 m downgradient are fairly similar, indicating large pH changes are typically restricted to the injection area. At buffered sites, the upgradient/background pH values are low, which is likely why buffer is added (**Figure 3.1d**). At buffered sites, the largest pH increases (positive ΔpH) occurs in wells close to the injection area, with smaller increases farther downgradient (**Figure 3.2d**).

The concentration of aqueous electron acceptors O_2 and NO_3^- were relatively low in upgradient wells (median = 0.3 mg/L O_2 and 0.1 mg/L NO_3-N) and consequently the decline in these parameters was small (**Table A-2**). There was little or no rebound in these parameters downgradient of the injection zone, presumably due to the low background concentrations.

Minimum upgradient (background) SO_4^{2-} concentrations varied widely from <1 mg/L to near the gypsum solubility limit (**Figure 3.1c**). In the injection area, SO_4^{2-} concentrations were reduced, typically by about 1 order of magnitude. However, SO_4^{2-} was not completely depleted at most sites. Further downgradient, the change in SO_4^{2-} concentration was smaller, indicating substantial attenuation of the low SO_4^{2-} plume (**Figure 3.2c**). SO_4^{2-} reduction did result in detectable increases in S^{2-} concentrations in the injection area and downgradient wells (**Figure 3.1e**). However, S^{2-} was only monitored in about 340 wells or 35% of the database wells, so care should be taken in extrapolating these results to other sites. In those wells where sulfide was monitored, the increase in sulfide was typically less than 1 mg/L (**Figure 3.2e**), although sulfide increased by more than 10 mg/L in a few injection area wells.

Maximum dissolved Fe, Mn, and arsenic concentrations observed in upgradient, injection area, and downgradient wells are shown in **Figures 3.1f**, **3.1h**, and **3.1i**. The maximum changes in Fe, Mn, and arsenic in individual wells are shown in **Figures 3.2f**, **3.2h**, and **3.2i**. The USEPA MCLs for these parameters are 0.3 mg/L Fe, 0.05 mg/L Mn and 0.01 mg/L arsenic. Substrate addition during ERB results in large increases in Fe concentrations in injection area wells, with smaller increases in downgradient wells (**Figure 3.2f**). At >50 m downgradient, the median increase in dissolved Fe is less than 1 mg/L. This indicates that iron is attenuating during downgradient migration.

Manganese concentrations exceeded the secondary MCL at 80% (48 of 61) of upgradient wells, 94% (118 of 125) injection area wells, and 76% (152 of 201) of downgradient wells (**Figure 3.1h**). Manganese concentrations in injection area wells were significantly elevated compared to upgradient concentrations. At the 10th through 90th percentiles, the injection area concentration was at least one order of magnitude higher than the corresponding upgradient concentration. The

range of manganese concentrations generally lessens with increasing distance downgradient. However, the highest downgradient manganese concentrations were fairly similar to the highest injection area manganese concentrations, indicating significant downgradient transport of dissolved manganese at some sites.

Arsenic was only monitored in 177 wells or 19% of the database wells, so care should be taken in extrapolating these results to other sites. Arsenic concentrations at injection area wells were elevated compared to upgradient concentrations (**Figure 3.1i**) indicating ED addition often results in an increase in injection area arsenic concentrations. The concentration ranges for the downgradient divisions are fairly similar to each other, though slightly decreasing with distance. For instance, the 50th percentile concentration is 0.014 mg/L for wells 0-10 m downgradient; 0.011 mg/L for wells 10-25 m downgradient; 0.0056 mg/L for wells 25-50 m downgradient; and 0.0056 mg/L for wells greater than 50 m downgradient. While the median arsenic concentrations for wells 25-50 m and greater than 50 m were lower than the MCL, a greater percentage of these wells exceeded the MCL (33% and 40%, respectively) than for upgradient wells (10%). These data indicate that arsenic mobilization could be a problem at distances greater than 50 m downgradient. However, it should be cautioned that there are very few monitoring points greater than 25 m downgradient (16 in total). In addition, all wells greater than 50 m downgradient are from a single site (Ft Devens, MA). Data from other sites would help verify if arsenic mobilization is an important concern. It should be noted that there is likely some selection bias in sites with arsenic data; that is, arsenic is most often monitored at sites where naturally occurring arsenic is known or expected to be present.

Figure 3.3 shows dissolved arsenic and dissolved iron concentrations in the same samples collected from injection area and downgradient monitoring wells, when concentrations of both Fe and arsenic were above the reporting limit. Increasing dissolved arsenic concentrations were highly correlated with increasing dissolved Fe concentrations ($p<0.01$), consistent with arsenic release during reduction of Fe oxides and/or arsenic removal during sorption/co-precipitation with Fe. At sites sampled for both arsenic and iron, very high dissolved Fe concentrations (i.e., greater than 200 mg/L) resulted in arsenic consistently above the MCL, while very low dissolved Fe concentrations (i.e., less than 0.5 mg/L) resulted in arsenic consistently below the MCL. As mentioned above, care should be taken when extrapolating this relationship since arsenic was not monitored at all sites, likely due to selection bias.
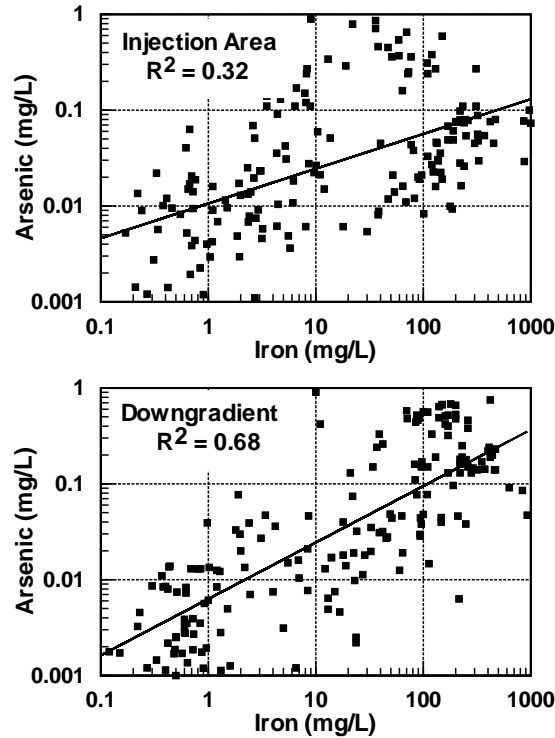
Figure 3.3. Arsenic versus iron concentrations for injection area and downgradient monitoring wells.

Maximum CH_4 concentrations at each well are shown in **Figure 3.1g**. The maximum change in CH_4 concentrations in individual wells are shown in **Figure 3.2g**. Upgradient CH_4 concentrations were substantially lower than injection area and downgradient concentrations at most percentiles due to methane production following organic carbon addition. The maximum increase in CH_4 concentration declines with distance, indicating some attenuation with distance. However, there were a significant number of wells at greater than 50 m downgradient with high CH_4 levels (>10 mg/L), indicating the potential for downgradient migration of dissolved CH_4.

3.5   POTABLE WATER IMPACTS

While SWQIs were detected in downgradient wells, the large majority of these wells were within the primary contaminant plume. At chlorinated ethene sites, only 31 of 380 downgradient wells (8%) did not contain at least one chlorinated ethene (PCE, TCE, *cis*-1,2-DCE, *trans*-1,2-DCE, 1,1-DCE , or vinyl chloride) above applicable MCLs. **Figure 3.4** shows the maximum concentrations of TOC, dissolved Mn, dissolved Fe, S^{2-}, and CH_4 at these wells; arsenic was not monitored at any of the wells. The concentrations of these SWQIs were generally within background levels. Where concentrations were much higher than background (e.g., TOC greater than 10 mg/L, CH_4 greater than 0.1 mg/L), these wells were generally located less than 10 m from the injection zone. The production of SWQIs is therefore unlikely to adversely impact potable water supplies.
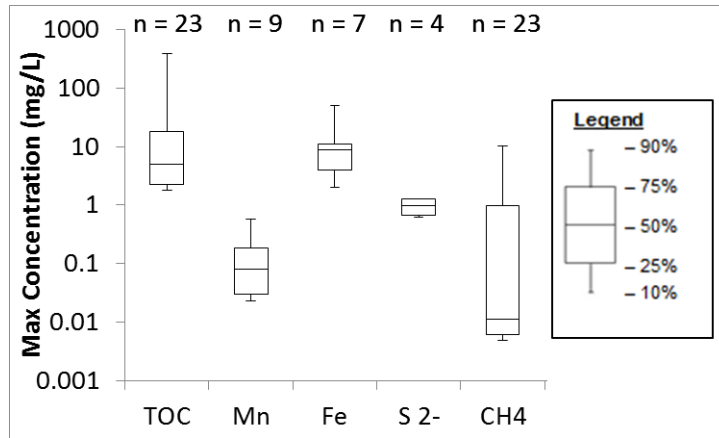
Figure 3.4. Box Plots of Maximum TOC, Dissolved Mn, Dissolved Fe, Dissolved S^{2-}, and Dissolved CH$_4$ in Wells without a Chlorinated Ethene Above Applicable MCLs.
Concentrations of SWQIs at these wells were generally within background ranges, indicating SWQIs will not further degrade potable water supplies.

4.0   SWQI INDICATOR SIMULATIONS

In this section, the formation and natural attenuation of SWQIs at ERB sites is illustrated using a numerical model developed to simulate the transport and consumption of DOC and multiple TEAs. This model employs the PE approach developed by Jakobsen and Postma (1999) and demonstrated by Curtis (2003). This approach assumes that the rate-limiting step is fermentation of DOC (i.e., releasing electron equivalents) and that other TEA reactions occur close to equilibrium. This model implementation is equivalent to organic carbon fully fermenting to H_2 and CO_2 at a determined rate, and then H_2 becoming consumed by multiple aqueous and mineral phase TEA processes controlled by their equilibrium constants. As shown by Curtis (2003), the PE approach has the advantage of avoiding thermodynamically unfavorable reactions and large errors in pH while allowing concomitant redox processes using multiple TEAs (Postma and Jakobsen, 1996; Jakobsen and Postma, 1999; Jakobsen et al., 1998).

4.1   MODEL FORMULATION AND INITIAL CONDITIONS

The model was used to simulate the fate of the added organic carbon and how the reduced products affected the aquifer over a period of 40 years following addition of emulsified vegetable oil (EVO) to form a PRB. The model domain is a two-dimensional cross-section of a water table aquifer extending 12 m vertically and 520 m horizontally. The active reaction zone examined with the model extends 260 m in the direction of flow. The barrier was represented as a 6 m deep by 15 m long by 65 m wide zone containing a total of 4,800 kiloequivalents (keq) of soybean oil ($C_{56}H_{100}O_6$) evenly distributed in the treatment zone (206 kilograms per meter barrier width). Soybean oil dissolution was simulated as a first-order process so that 77% of the residual soybean oil was released to groundwater as DOC in 6.9 years. This scenario results in essentially all of the soybean oil being released to the aqueous phase in 22 years.

DOC degrades by releasing electrons that react with TCE and also with other TEAs including O_2, sediment Mn[IV], sediment Fe[III], SO_4^{2-}, and CO_2 producing CH_4. The reaction between released electrons and TEAs was simulated as an equilibrium reaction. The rate of DOC consumption (r_1) was simulated as

$$r_1 = -k_1 * C_{DOC} - k_2 * C_{DOC} * C_{TCE}$$

where

$$
\begin{aligned}
C_{DOC} &= \text{DOC concentration (mM)} \\
C_{TCE} &= \text{TCE concentration (mM)} \\
k_1 &= 1^{st} \text{ order DOC decay rate} \\
k_2 &= 2^{nd} \text{ order DOC and TCE decay rate}
\end{aligned}
$$

In the partial equilibrium framework, Fe[III] is treated as an equilibrium phase mineral. Dissolution of amorphous $Fe(OH)_3$ and goethite (FeOOH) occur by the reactions:

$$Fe(OH)_3 + 3H^+ \longleftrightarrow Fe^{3+} + 3H_2O \qquad pK_{SP} = 4.9$$

and

$$FeOOH + 3H^+ \longleftrightarrow Fe^{3+} + 2 H_2O \qquad pK_{SP} = -1.0$$
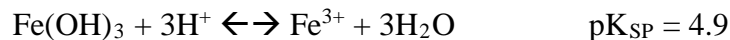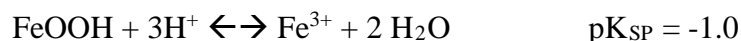
At many sites, Fe[III] will be present as mixtures of amorphous $Fe(OH)_3$, goethite, and other minerals. As a result, the effective solubility product (pK_{SP}) for Fe[III] in any aquifer is unknown, but is expected to be somewhere between 4.9 and -1.0, values representative of readily dissolved and more stable Fe oxide forms, respectively. A pK_{SP} value of 0.239 was used in this simulation based on model calibration results from the Bemidji site and evidence from numerous ERB sites of simultaneous iron reduction and methanogenesis, which does not occur when higher dissolution pK_{SP} values are applied. Dissolved Fe[II] and Mn[II] were assumed to undergo cation exchange with sediments and precipitation as siderite ($FeCO_3$) and rhodochrosite ($MnCO_3$). Magnetite precipitation was not considered in these simulations based on limited magnetite production at Bemidji.

CH_4 produced by fermentation coupled to methanogenic degradation initially enters the dissolved phase. Once the sum of partial pressures of all dissolved gasses ($P_{CH4} + P_{CO2} + P_{N2}$) reaches hydrostatic pressure, CH_4 and other gases are assumed to outgas to the vadose zone. In the field, outgassing is expected to occur in relatively coarse grained sediments where the gas bubbles can migrate upward through the sediment pores. In finer grained sediment, gas bubbles can remain trapped within the pores by capillary forces. Once CH_4 production slows, the CH_4 in these trapped bubbles could potentially dissolve back into groundwater and be carried downgradient with ambient groundwater flow. In the simulations presented here, all excess CH_4 is outgassed and there are no trapped bubbles that redissolve.

The model was run for a total of 40 years. The added soybean oil is depleted in 22 years so most of the SWQIs are produced during the 0 – 22 year period and then during the 22 – 40 year period the aquifer plume continues to evolve and slowly recover. The initial water and aquifer chemistry for the model is based roughly on that of the Bemidji crude oil spill site (**Table 4.1**). The model is homogeneous and isotropic with the groundwater flow velocity set to 0.06 m/day.

TABLE 4.1.
Initial Condition and Background Concentrations [mM] of Inorganic Aqueous Species and Sediment Electron Acceptors.

	Conc. (mM)		Conc. (mM)
DIC (1 mM = 12 mg/L)	3.65	CH_4 (1 mM = 16 mg/L)	0.0
Ca^{2+} (1 mM Ca = 40 mg/L)	1.24	Cl^- (1 mM = 35 mg/L)	0.31
Fe^{2+} (1 mM = 56 mg/L)	5.1E-21	Mg^{2+} (1 mM = 24 mg/L)	0.59
Na^+ (1 mM = 23 mg/L)	0.077	O_2 (1 mM = 32 mg/L)	0.25
Mn^{2+} (1 mM = 55 mg/L)	0	SO_4^{2-} (1 mM = 96 mg/L)	1.56
N_2 (inert) (1 mM = 28 mg/L)	0.45	pH	7.6
Sediment Fe[III] (bioavailable)	0.98 g/kg	pe	14.3
Cation Exchange Capacity (CEC)	47.5 mM/L aquifer volume	Sediment Mn[IV]	0.03 g/kg

4.2   SIMULATION RESULTS

The model results are displayed in **Figures 4.1** and **4.2** as snapshots of the plume after 5, 15, and 30 years. The time point at 5 years was chosen to display the SWQI plume that develops as a result of the ERB emplacement. The 15-year figure displays conditions when the soybean oil is almost exhausted. At this time, the migration of the SWQI plume is apparent, but the waning of the soybean oil source is also clear, especially near the treatment zone. The final time point of 30 years is used to convey the progress of the recovery of the aquifer from the reduced conditions created by the remediation.

Figure 4.1 shows the spatial distribution of DOC, DO, pH, SO_4, and CH_4 at 5, 15 and 30 years. The assumed first order dissolution rate for residual soybean oil results in 65% being dissolved by 5 years and consumption of all the soybean oil after 22 years. Significant concentrations of DOC are restricted to the area containing residual soybean oil, so CH_4 production is also restricted to this area.

A plume of depleted O_2 extends over 100 m from the treatment zone by 5 years and at 15 years extends beyond 250 m. Although recovery of the aquifer begins at 22 years, increased O_2 is visible only at the base and top of the model plume at 30 years. The slow recovery of O_2 is due to the large reservoir of sorbed Fe[II] on the sediments that consumes O_2 transported from upgradient.   In sulfate-rich aquifers, FeS may form but is not expected to slow recovery because the mineral surface becomes oxidized which restricts further oxidation of the underlying FeS. A similar slow recovery of an aquifer has been observed at the Cape Cod research site where treated wastewater entered the aquifer through infiltration beds for 56 years (Repert et al., 2006). While NO_3^- was not included in the model simulation, NO_3^- is expected to behave similarly to O_2 with slow recovery until the soybean oil and Fe[II] are depleted.

A plume of slightly lower pH water migrates from the source zone. After 5 years the pH plume extends over 100 m from the source, and at 15 years it extends beyond 250 m. Slightly higher pH values can be seen in the iron-reducing zone due to consumption of protons by the reaction of DOC oxidation coupled to iron reduction. The 30-year time point shows that once the soybean oil source is exhausted, pH in the aquifer recovers as clean groundwater moves in from upgradient. Note that the simulated pH changes are less than one unit and may not be detectable because of the typically sparse coverage of monitoring wells. The pH is buffered by excess calcite and cation exchange of H^+ with aquifer minerals. More details on the reactions controlling pH can be found in Ng et al. (2015).

Immediately after addition of the soybean oil, SO_4^{2-} is depleted within the source zone. The zone of depleted SO_4 extends approximately 50 m from the source zone after 5 years and approximately 75 m from the source zone after 15 years. Lower SO_4^{2-} concentrations are observed up to approximately 140 m downgradient after 30 years; however, these levels are not as depleted as those closer to the injection area in earlier time periods. In addition, after 30 years SO_4^{2-} concentrations in and around the source area began to recover as upgradient, sulfate-rich groundwater fluxes into the area. Recovery of SO_4^{2-} is much faster than O_2 since much more strongly reducing conditions are required for sulfate reduction.
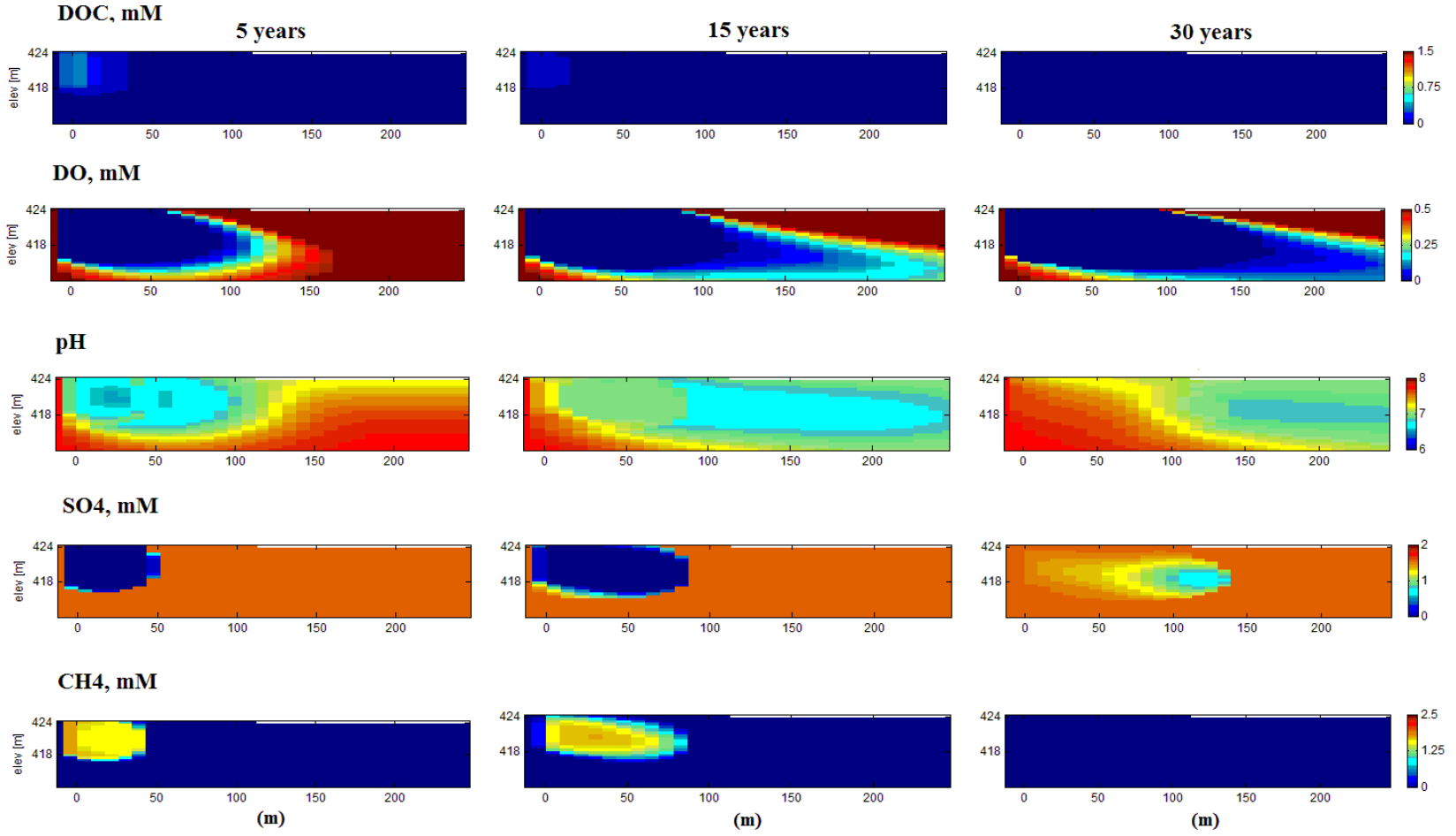
Figure 4.1. Simulated Dissolved Organic Carbon (DOC), Dissolved Oxygen (O$_2$), pH, Sulfate (SO$_4$) and Dissolved Methane (CH$_4$) Concentrations at 5, 15 and 30 Years after Substrate Addition. DOC, DO, SO$_4$, and CH$_4$ concentrations are in units of mM.
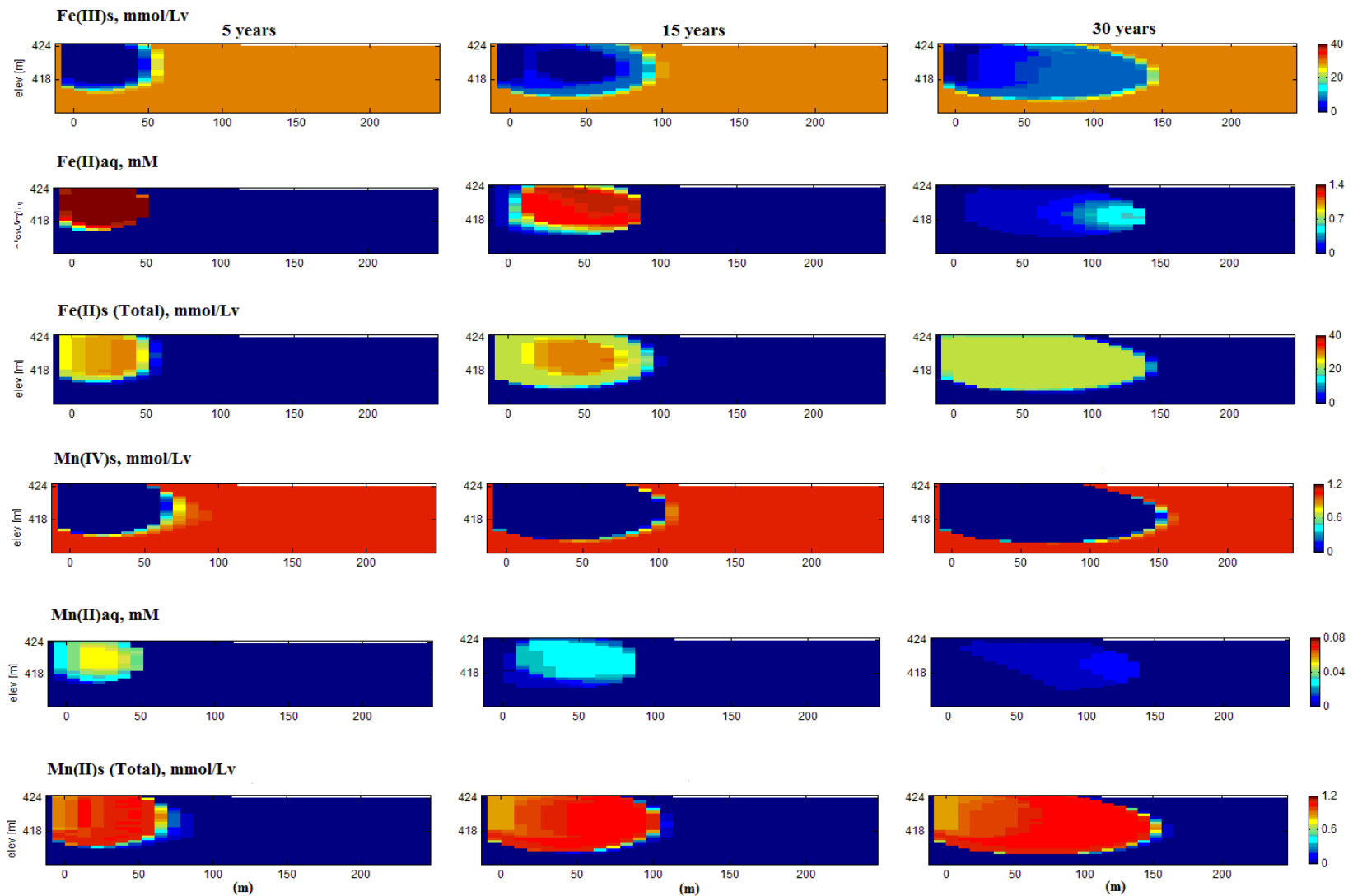
Figure 4.2. Simulated Sediment Fe[III], Dissolved Fe^{2+}, Sediment Fe[II], Sediment Mn[IV], Dissolved Mn^{2+}, and Sediment Mn[II] at 5, 15 and 30 years after Substrate Addition. Fe^{2+} and Mn^{2+} concentrations are in units of mM. Sediment Fe[III], Fe[II], Mn[IV] and Mn[II] concentrations are in units of mmol per liter aquifer volume.

30

Methane production begins immediately after emplacement of the soybean oil and by 5 years a CH_4 plume extends over 50 m from the source. By this time, the total gas pressure in the treatment zone has exceeded hydrostatic pressure and outgassing has started. By 15 years, the dissolved CH_4 plume extends almost 100 m from the source. The early establishment of anaerobic conditions in the aquifer after the start of treatment restricts aerobic CH_4 oxidation to small areas on the fringe of the plume. Even after all the soybean oil has been depleted, CH_4 consumption with oxygen is limited to a zone of low O_2 and low CH_4 that separates these two plumes.

In this simulation, CH_4 is assumed to be capable of driving reduction of sediment Fe[III] based on field monitoring results at the Bemidji site. If this occurs, then iron reduction will be the main process limiting the growth of the dissolved CH_4 plume. However, if adapted microorganisms capable of reducing Fe[III] using CH_4 are not present, dissolved CH_4 will migrate downgradient with little attenuation beyond dispersive mixing. Once the primary organic substrate (soybean oil) is exhausted, CH_4 production stops. If essentially all of the gaseous CH_4 has been released to the vadose zone, dissolved CH_4 concentrations are expected to decline relatively quickly. However, if significant amounts of gaseous CH_4 are trapped below the water table, dissolution of these trapped bubbles could maintain the dissolved CH_4 plume for some time.

Dissolved Fe^{2+} and Mn^{2+} and sediment Fe[III], Fe[II], Mn[IV] and Mn[II] are shown in **Figure 4.2**. Sediment Fe[II] and Mn[II] includes both material attached to cation exchange sites on the sediment surfaces and material precipitated as carbonate minerals (siderite and rhodochrosite).

After 5 years much of the sediment Fe[III] is depleted in the source zone, releasing dissolved Fe^{2+} to the aqueous phase. However, downgradient migration of dissolved Fe^{2+} is delayed behind the low O_2 plume by cation exchange to the sediments. Dissolved Fe^{2+} concentrations reach over 1 mM while sediment Fe[II] reaches ~ 30 mM showing that most of the reduced iron is bound to the sediment. Over time, the simulated zone of depleted sediment Fe[III] grows since the model assumes these minerals can be reduced by dissolved CH_4. After all of the DOC has degraded, the large reservoir of sorbed Fe[II] remains steady and does not readily desorb. At 30 years, the recovery of the aquifer is apparent as the dissolved Fe[II] plume disperses and siderite redissolves, but these two forms make up a relatively small fraction of the total reduced Fe. As clean aerobic groundwater enters from upgradient, Fe[II] desorbs from the sediment, mixes with O_2, and re-precipitates as Fe[III]. During the 40-year simulation, about 25% of bioavailable Fe[III] in the 520-m model domain is reduced, but the percentage is far higher in the injection zone (~90%).

Overall, Mn behaves similarly to Fe with Mn[IV] reduced to dissolved Mn^{2+} in the source area, and downgradient migration of Mn^{2+} limited by cation exchange on the sediments. The total amount of Mn[II] produced is much lower than Fe[II] due to the much lower amount of Mn[IV] originally present in the sediment. This is consistent with results from the SWQI database which show Mn^{2+} levels are often significantly lower than Fe^{2+}. The zone of depleted Mn[IV] is projected to grow more rapidly than the Fe[III] depleted zone because Mn can be reduced under relatively more oxidizing conditions than Fe. Similar to Fe, downgradient migration of dissolved Mn^{2+} is limited by cation exchange to the sediments and the dissolved Mn^{2+} dissipates once the soybean oil is depleted.

Figure 4.3 shows the distribution of electron (e⁻) equivalents released over time in the entire model domain as soybean oil dissolves releasing DOC, which is then fermented reducing TCE, O_2, Mn, Fe, SO_4^{2-}, and producing CH_4. Over the first 15 years, the very large majority of e⁻ equivalents are used to reduce Fe[III] to Fe[II], SO_4^{2-} to S^{2-}, and CO_2 to CH_4. Overall, electrons consumed in O_2, Mn and TCE reduction are minor contributors to the electron balance. After 22 years, the fraction of e⁻ equivalents associated with CH_4 reduction declines slightly with a tiny increase in Fe[II] as CH_4 reduces Fe[III] in the downgradient aquifer. As discussed above, reduction of Fe[III] by CH_4 depends of the presence of specialized microorganisms that facilitate this process and probably does not occur at some sites.
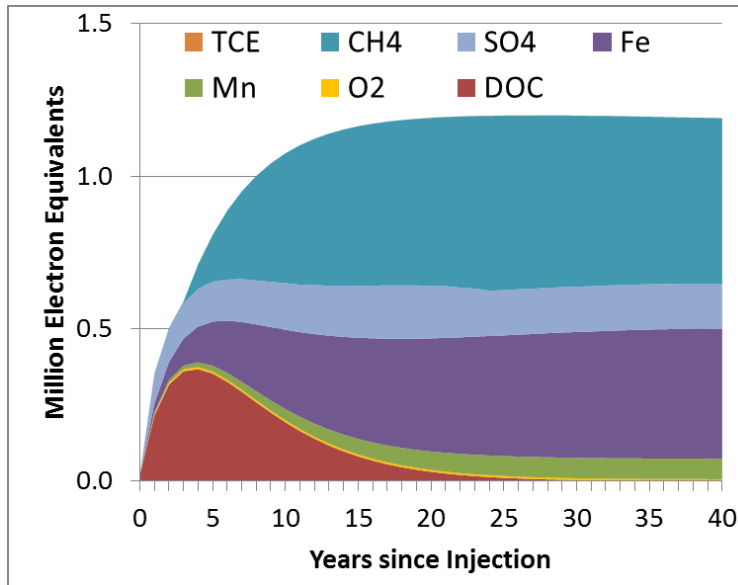
Figure 4.3. Simulated Distribution of Cumulative Electron Equivalents over Time Following Soybean Oil Addition to Stimulate ERB. The contributions of the electron acceptors are represented by the vertical heights of their color bands at each time. Electron equivalents are calculated over the first 250 m downgradient of the injection point. The electron equivalents used for TCE reduction are too low to be visible on the scale of the plot.

In summary, iron reduction and methanogenesis are expected to be major electron sinks in many aquifers. In aquifers with high levels of SO_4^{2-}, sulfate reduction will also be a major sink. Much of the Fe[II] and Mn[II] produced is expected to remain immobilized on the aquifer material and is not expected to migrate long distances downgradient. Similarly, essentially all of the sulfide will precipitate with available metals with little to no sulfide migration downgradient. If appropriate microorganisms are present, anaerobic methane oxidation using Fe[III] as an electron acceptor can limit the downgradient migration of dissolved CH_4. However these organisms may not be present, resulting in dissolved CH_4 migrating substantial distances downgradient. Once the fermentable organic carbon is depleted, CH_4 production will stop and the dissolved CH_4 plume is expected to dissipate.

5.0 CONCEPTUAL MODEL OF SWQI PRODUCTION AND ATTENUATION

During ERB, large amounts of easily fermented organic substrates are added to the target treatment area to degrade or immobilize the COCs. These substrates are fermented to H_2, acetate, and other VFAs that are then consumed in microbially mediated reactions that consume O_2, NO_3^-, and SO_4^{2-} as well as Fe[III] and Mn[III/IV] containing minerals, creating a 'plume' of SWQIs. Fortunately, this 'plume' of impacted groundwater is usually confined within the original contaminant plume and is unlikely to adversely impact potable water supplies.

Figure 5.1 shows a typical pattern of SWQI parameters with time in the: 1) injection area; 2) near plume (25 m downgradient); 3) medium-distance plume (50 m downgradient) and 4) far plume (100 m downgradient). Readers should note that the trends shown in **Figure 5.1** may not occur at all sites and broad ranges of SWQI parameter concentrations have been observed. The time period for production and attenuation of SWQIs can vary from 10 to over 100 years, depending on the amount and duration of substrate addition, groundwater transport velocity, and concentrations of background electron acceptors.

Organic substrate addition results in a rapid increase in TOC in injection area monitoring wells, with maximum TOC concentrations typically ranging from 50 to 500 mg/L. However, much higher TOC concentrations are observed at some sites. TOC concentrations often remain high for several years in the injection area due to the use of slow release electron donors (e.g., EVO) and/or repeated substrate injections, and then decline once substrate addition ends. However, low levels of TOC may continue to be released from endogenous decay of accumulated biomass (Sleep et al., 2005; Adamson and Newell, 2009). Increases in carbon loading are expected to result in greater SWQI formation. However, these SWQIs will attenuate with time and distance downgradient. Reducing the carbon loading to reduce SWQI production may reduce treatment efficiency, possibly resulting in greater exposure to chlorinated solvents and other contaminants.

Maximum TOC concentrations in downgradient wells are generally much lower than in the injection area, indicating TOC in the aqueous phase is rapidly consumed and does not migrate long distances downgradient. The rapid consumption of TOC in the injection area is due to reactions with background electron acceptors (e.g. O_2, NO_3^-, Mn[IV], Fe[III], SO_4^{2-}), the target contaminants, and fermentation to CH_4. Since TOC is largely restricted to the area in and immediately downgradient of injection area, these redox reactions are also largely restricted to the same area. Thermodynamic calculations indicate that reduction reactions should proceed in the order of O_2, NO_3^-, Mn[IV], Fe[III], SO_4^{2-}, and CO_2. However, these processes often overlap (e.g., methane production occurring before complete sulfate reduction) due to spatial variability, energy limitations from low reactant concentrations, slow reaction kinetics, and addition of excess electron donor (Cozzarelli et al., 2000; Curtis 2003; Jakobsen and Postma 1999).
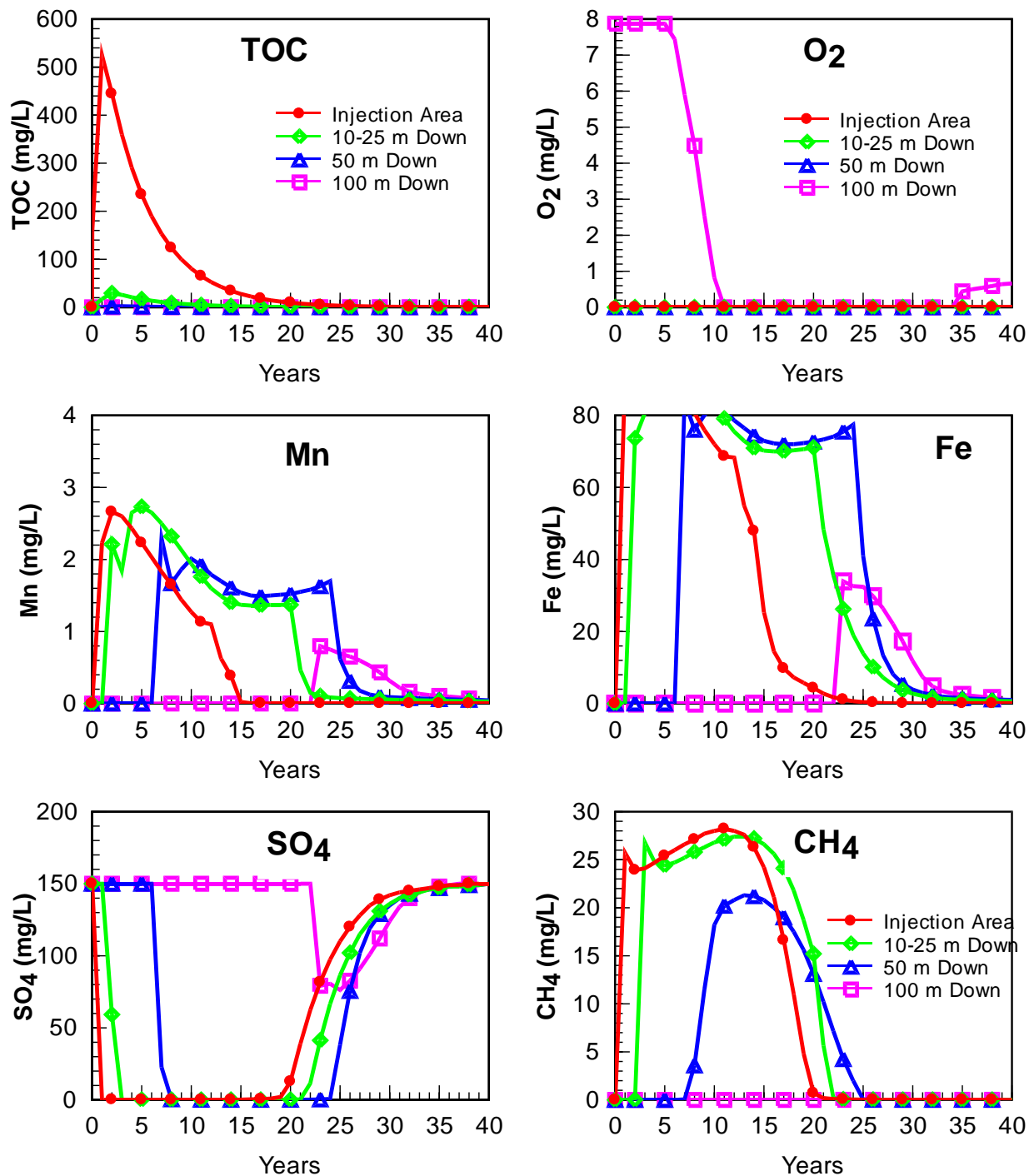
Figure 5.1. Typical Variation in SWQI Parameters over Time with Distance from Injection. Graphs compare concentrations at wells in the injection area and 25 m, 50 m, and 100 m downgradient for 40 years post-injection.

Declines in pH are often observed during ERB due to the release of VFAs and carbonic acid (H_2CO_3) from substrate fermentation and hydrochloric acid (HCl) from dechlorination reactions. In general, naturally occurring carbonate minerals are not an effective pH buffer, since high

34

concentrations of dissolved CO_2 produced during ERB prevent carbonate mineral dissolution (Kouznetsova et al. 2010). In some cases, pH declines can be limited by alkalinity released during the reduction of nitrate, manganese and iron oxyhydroxides, and by CO_2 degassing. If sufficient alkalinity is released, increases in pH may be observed.

In the injection area, O_2 and NO_3^- decline rapidly following substrate addition and often remain low for years after TOC declines due to reduction of O_2 and NO_3^- by sediment organic carbon and/or reduced minerals. Concentrations of O_2 and NO_3^- in downgradient wells decline with the arrival of oxygen- and nitrate-depleted water. In most cases, there is little or no increase in O_2 or NO_3^- with distance downgradient due to the very limited mixing between the anaerobic plume and background aerobic groundwater (Borden and Bedient 1986; Schirmer et al. 2001).

Similar to O_2 and NO_3^-, SO_4^{2-} concentrations decline in the injection area following substrate addition. However, biodegradation coupled to sulfate reduction is less energetically favorable than biodegradation coupled to O_2, NO_3^-, Mn[IV], and Fe[III] reduction. As a result, SO_4^{2-} is depleted more slowly than these other TEAs and substantial amounts of SO_4^{2-} may persist in the injection area if background SO_4^{2-} levels are high. In downgradient wells, SO_4^{2-} concentrations decline with the arrival of anaerobic, low SO_4^{2-} groundwater. However, the decline in sulfate in downgradient wells is somewhat more limited than in the injection area, presumably due to release of SO_4^{2-} exchanged onto variably charged sediment surfaces (Bolan et al., 1986; Guadalix and Pardo, 1991). Once injection area TOC declines, SO_4^{2-} is expected to recover more rapidly than O_2 or NO_3^- since reduced iron and manganese minerals will not reduce sulfate.

Sulfate reduction results in the production of S^{2-} which combines with protons (H^+) producing hydrogen sulfide (H_2S). H_2S is a colorless, poisonous, inflammable gas with the characteristic 'rotten egg' smell which is detectable at 0.01 ppm (USEPA 2010). In most aquifers, substantial amounts of naturally occurring Fe are present and most of the H_2S produced will rapidly precipitate as insoluble iron sulfide minerals (FeS or FeS_2; Cozzarelli et al. 1999). However, detectable levels of sulfide (~1 mg/L) are often observed in injection areas, expecially when background SO_4^{2-} levels are high. In the isolated cases where SO_4^{2-} concentrations are high and solid phase Fe is low, some dissolved sulfide may migrate a short distance downgradient before reacting or precipitating.

High concentrations of sulfide can inhibit reductive dechlorination, reducing bioremediation effiency. Hoelen and Reinhard (2004) reported that 400 mg/L Na_2S inhibited TCE, DCE, and VC degradation. Sung (2005) found that 64 mg/L total sulfide inhibited growth of d*esulfuromonas michiganensis strain BB1, sulfurospirillum multivorans, desulfitobacterium sp. strain Viet1, and dehalococcoides sp. strain FL2 and strain BAV1*. However at low concentrations (<16 mg/L as S), sulfide does not inhibit dechlorinators (Löffler et al., 2005). At most sites, sulfide levels are well below levels that would inhibit reductive dechlorination. However, inhibitory levels of sulfide were observed at one site where upgradient sulfate concentrations were very high (~5000 mg/L) and bioavailable iron was very low (<11 mg/kg) (Keener et al., 2012).

Many aquifer sediments contain significant levels of Fe[III] and Mn[III/IV] oxyhydroxides. Fe[III] is commonly present as mixtures of poorly crystalline amorphous Fe[III] oxyhydroxides and more crystalline forms. Solid-phase Fe data compiled from 20 contaminated aquifers showed bioavailable Fe varied approximately 3 orders of magnitude from 0.01 g/kg to over 17

g/kg and total iron varied from 0.2 to 110 g/kg (Borden et al., 2015). Mn is most commonly present as metastable Mn[IV] and Mn[III] hydrous oxides, characterized by structural defects, domain intergrowths, cation vacancies, and solid solutions (Villalobos et al. 2003). The Mn[III/IV] concentration in soils and aquifer sediments (median = 0.02 g/kg; Chen et al., 1999) is often much lower than the iron concentration.

During ERB, increased levels of H_2 and VFAs produced from substrate fermentation lead to reduction of Fe[III] and Mn[III/IV] oxyhydroxides and release of dissolved Fe^{2+} and Mn^{2+}. Early research suggested that the poorly crystalline forms of Fe[III] (e.g., ferrihydrite) could be rapidly and completed reduced (Lovley and Phillips 1986) while reduction of more crystalline forms (e.g., goethite and hematite) was more limited (Lovley and Phillips, 1987). However, more recent work has shown that a variety of crystalline Fe-oxides can be reduced by ERB (Roden and Zachara, 1996; Roden et al., 2000; Roden and Urrutia, 2002). Mn[II] can be generated by dissimilatory reduction of Mn(III/IV) hydrous oxides on sediments by microorganisms (Tebo et al., 2004) or by abiotic reduction of these oxides by Fe[II] (Postma and Appelo, 2005). In some aquifers, Mn and Fe concentrations have been observed to decline before TOC is depleted, presumably due to depletion of bioavailable Mn[III/IV] and Fe[III] in the injection area aquifer material. Once TOC levels decline in the injection area, production of additional Mn[II] and Fe[II] will slow, and dissolved Mn and Fe concentrations in monitoring wells should start to decline.

Much of the reduced Fe[II] produced during ERB will be retained on the aquifer material within the injection area through a variety of processes including ion exchange and surface complexation reactions (Davis and Kent, 1990; Baeyens and Bradbury, 1997; Davis et al. 1998) and formation of mixed Fe[II/III] phases such as magnetite and green rust and pure Fe[II] phases like siderite (Frederickson et al., 1998; Hansel et al. 2005). Mn[II] is not expected to precipitate as most sites, but can be retained by sorption processes when concentrations of competing cations are low and the pH is alkaline (Baeyens and Bradbury, 1997). However, ERB often results in reduced pH with high concentrations of Fe^{2+} which will minimize Mn^{2+} retention in the injection area aquifer material.

Fe[II] and Mn[II] that is not retained within the injection area will migrate downgradient with natural groundwater flow. During downgradient migration, a portion of the dissolved Mn and Fe will sorb to the aquifer material, reducing the maximum concentrations observed in downgradient wells. Over time, Fe^{2+} and Mn^{2+} production in the source area will decline, and these sorbed materials could potentially be released to the aqueous phase. However, the desorption rate will be limited by the supply of exchangeable cations entering the plume from upgradient. Numerical model simulations of oxygen recovery in an anaerobic wastewater plume in Cape Cod, MA indicate that the maximum concentrations of dissolved Fe and Mn released will be much lower than peak concentrations observed during the substrate loading phase (Ng 2015).

Arsenic is naturally present in many aquifers, often co-precipitated and/or sorbed to iron and aluminosilicate minerals (Pierce and Moore, 1982; Smedley and Kinniburgh, 2002; Kent and Fox, 2004). The general term sorption is used to encompass all binding mechanisms of arsenic to Fe[III] phases. Under oxidizing conditions, As[V] is the dominant form and is present in solution as a negatively charged ion ($H_2AsO_4^-$ or $HAsO_4^{2-}$). Under mildly reducing conditions, As[III] is the dominant form and occurs as an uncharged species ($As(OH)_3^0$). Typically, As[III]

sorbs less strongly than As[V] on minerals except Fe[III] oxides and oxyhydroxides (Dzombak and Morel, 1990; Dixit and Hering, 2003).

During ERB, sorbed arsenic is released to solution when As[V] is reduced to As[III] and Fe[III] is reductively dissolved (Kent and Fox, 2004; Höhn et al., 2006; Hering et al., 2009; He et al., 2010; Cozzarelli et al., 2015). As Fe-rich groundwater migrates downgradient, Fe[II] sorbs to the sediment or precipitates as Fe-bearing minerals (FeS, carbonates, magnetite) and aqueous Fe concentrations decline. The available monitoring data suggest that arsenic follows a similar pattern and aqueous arsenic concentrations decline as the anaerobic plume migrates downgradient and encounters Fe[III]-rich sediments. While oxidation of aqueous As[III] to As[V] is a kinetically slow process, As[III] can sorb to amorphous ferrihydrite (am-Fe(OH)$_3$) and then undergo much more rapid heterogeneous oxidation (i.e., oxidation at an iron-mineral surface), generating strongly sorbed As[V] (Pierce and Moore, 1982; Smedley and Kinniburgh, 2002). Once TOC concentrations in the injection area decline, Fe[III] and As[V] reduction is expected to decline with a concurrent decline in arsenic release. At sites where concentrations of sediment-bound As[V] are low, minimal arsenic will be released.

TOC fermentation products (H$_2$ and acetate) in the injection area that are not consumed in microbially mediated reactions with contaminants or background electron acceptors will be fermented to CH$_4$, which can result in high CH$_4$ concentrations in the injection area and downgradient aquifer (Jacob et al., 2005; Riis et al., 2007). In saturated media, if the sum of gas partial pressures exceeds the hydrodynamic pressure, the gases will come out of solution and form bubbles (Amos and Mayer, 2006). This occurs primarily near the water table due to the lower hydrostatic pressure. At greater depths, groundwater can appear to be supersaturated with CH$_4$ due to the higher pressure. In relatively homogeneous, coarse grained sediments, gas bubbles can migrate upward into the vadose zone, removing CH$_4$ from the aquifer. However, in finer grained sediments upward migration of gas bubbles will be more limited. If the gas bubbles are not released to the vadose zone, they will eventually dissolve, releasing CH$_4$ back into groundwater.

Field monitoring at ERB sites has shown that CH$_4$ levels can be elevated in the headspace of injection area wells, while CH$_4$ levels in soil gas measurements collected just below the land surface are typically lower (TSI and Solutions-IES, 2003). This is due to diffusive mixing with O$_2$ from the land surface and subsequent oxidation by methanotrophs (Fischer et al., 1996; Amos et al., 2005; Ma et al., 2012; Warren et al., 2014). However, CH$_4$ can be released to the land surface or subsurface structures when methane production rates are high and oxygen transport through the vadose zone is restricted by saturated soil conditions (Sihota et al., 2013).

Dissolved CH$_4$ produced in the injection area will migrate downgradient with groundwater flow and could potentially biodegrade if the CH$_4$ plume mixes with aerobic groundwater. However, the actual extent of aerobic CH$_4$ biodegradation in the saturated zone will be limited by an anoxic zone that develops between the strongly anaerobic water containing CH$_4$ and the oxygenated background groundwater (Borden and Bedient 1986, Amos et al. 2005). Recent research indicates that methane could be consumed using NO$_3^-$ (Raghoebarsing et al., 2006), Mn and Fe oxides (Beal et al., 2009; Crowe et al., 2011; Amos et al. 2012) and SO$_4^{2-}$ (Caldwell et al., 2008; Grossman et al., 2002) as TEAs. These anaerobic TEAs are potentially very important since they could limit the downgradient migration of CH$_4$ plumes. However anaerobic methane oxidation requires a consortium of archaea and bacteria (Boetius et al., 2000) and has a very low

energy yield (Caldwell et al., 2008). As a result, anaerobic methane oxidation reactions may be slow or may not occur at some sites, and dissolved CH_4 can migrate long distances in some aquifers. Once TOC in the injection area declines, CH_4 production will stop and dissolved CH_4 should be transported downgradient by groundwater flow.

6.0   RESEARCH IMPLICATIONS AND OPPORTUNITIES

At most sites, the majority of the ED added to the aquifer is consumed in the reduction of Fe[III] to Fe[II], SO_4^{2-} to S^{2-}, and CO_2 to CH_4. At many sites, anaerobic methane oxidation using Fe[III] and SO_4 as TEAs is expected to be the primary attenuation mechanism for dissolved CH_4, resulting in further production of Fe[II] and S^{2-} at many sites. The very large majority of Fe[II] and S^{2-} produced is retained on the aquifer material, generating a large reservoir of reducing power within the aquifer.

Monitoring data and modeling studies at the Cape Cod, MA wastewater plume indicate that a portion of the added organic carbon is retained on the aquifer material as BMSOC. The BMSOC is a small fraction of sediment organic carbon and oxidation of BMSOC appears to be slow. However, this BMSOC may greatly delay re-oxidation of the aquifer and has the potential to generate reducing conditions that support further Fe[II] reduction.

These large reservoirs of reduced iron and sulfur minerals and organic carbon will cause the aquifer downgradient of ERB projects to remain anoxic to reducing for years to decades after the end of substrate addition. However, these reservoirs of Fe[II], reduced S, and organic carbon also have the potential to increase degradation and/or attenuation rates for a variety of groundwater contaminants including chlorinated solvents, explosives and propellants (TNT, RDX, HMX, ClO_4^-), NO_3^-, chromate, and selected radionuclides (TcO_4^-, UO_2^{2+}) (Butler and Hayes, 1998; Lee and Batchelor, 2002, 2003; Ferry et al., 2004; Sleep et al., 2005; AFCEE, 2008; He et al., 2009; Adamson and Newell, 2009). Additional research is needed to better understand the impact of these reduced materials on contaminant degradation/attenuation rates.

7.0   REFERENCES

Abrams, R. H., Loague, K., and Kent, D. B., 1996. Development and testing of a compartmentalized reaction network model for redox zones in contaminated aquifers. Water Resourc. Res. 34: 1531-1541.

Adamson D. T. and Newell, C.J., 2009. Support of source zone bioremediation through endogenous biomass decay and electron donor recycling. Bioremed. J. 13: 29-40.

AFCEE (Air Force Center for Engineering and the Environment), NFESC (Naval Facilities Engineering Service Center), ESTCP (Environmental Security Technology Certification Program), 2004. Principles and Practices of Enhanced Anaerobic Bioremediation of Chlorinated Solvents. Prepared by Parsons Infrastructure & Technology Group, Inc., Denver, CO, USA.

AFCEE, 2008. Workshop on *In Situ* Biogeochemical Transformation of Chlorinated Solvents, February 2008.

Albrechtsen, H.-J., Heron, G. and Christensen, T. H., 1995. Limiting factors for microbial Fe(III)-reduction in a landfill leachate polluted aquifer (Vejen, Denmark). FEMS Microbiology Ecology 16: 233-248.

Amos, R. T., Mayer, K. U., Bekins, B. A., Delin, G. N. and Williams, R. L., 2005. Use of dissolved and vapor-phase gases to investigate methanogenic degradation of petroleum hydrocarbon contamination in the subsurface. Water Resourc. Res., 41, W02001, doi:10.1029/2004WR003433.

Amos, R. R. and Mayer, M. K., 2006. Investigating the role of gas bubble formation and entrapment in contaminated aquifers: Reactive transport modelling. J. Contam. Hydrol. 87: 123-154.

Amos, R. T., Bekins, B. A., Cozzarelli, I. M., Voytek, M. A., Kirshtein, J. D., Jones, E. J. P. and Blowes, D.W., 2012. Evidence for iron-mediated anaerobic methane oxidation in a crude oil-contaminated aquifer. Geobiology 10: 506-517.

Baedecker, M.J., I.M. Cozzarelli, D.I. Siegel, P.C. Bennett, and R.P. Eganhouse, 1993. Crude oil in a shallow sand and gravel aquifer–III. Biogeochemical reactions and mass balance modeling in anoxic ground water, Appl. Geochem. 8: 569–586.

Baeyens, B. and Bradbury, M. H., 1997. A mechansitic description of Ni and Zn sorption on Na-montmorillonite. 1. Titration and sorption measurements. J. Contam. Hydrol. 27: 199-222.

Beal, E. J., House, C. H. and Orphan, V. J., 2009. Manganese- and iron-dependent marine methane oxidation. Science 325(5937): 184-187.

Bethke C. M., Sanford R. A., Kirk M. F., Jin Q. and Flynn T. M., 2011. The thermodynamic ladder in geomicrobiology. Am. J. Sci. 311: 183-210.

Boetius, A., Ravenschlag, K., Schubert, C. J., Rickert, D., Widdel, F., Gieseke, A., Amann, R., Jorgensen, B. B., Witte, U. and Pfannkuche, O., 2000. A marine microbial consortium apparently mediating anaerobic oxidation of methane. Nature 407(6804): 623-626.

Bolan, N. S., Scotter, D. R., Syers, J. K., and Tillman, R. W., 1986. The effect of adsorption on sulfate leaching. Soil Sci. Soc. of America J. 50: 1419-1424.

Borden, R. C. and Bedient, P. B., 1986. Transport of dissolved hydrocarbons influenced by reaeration and oxygen limited biodegradation: 1. Theoretical development. Water Resourc. Res. 22: 1973-1982.

Borden, R. C., Tillotson, J. M., Ng, G.-H. C., Bekins, B. A., Kent, D. B., and Curtis, G. P., 2015. Extent and Persistence of Secondary Water Quality Impacts after Enhanced Reductive Bioremediation. Strategic Environmental Research and Development Program, Arlington, VA, www.serdp-estcp.org.

Butler, E. C. and Hayes, K. F., 1998. Effects of solution composition and pH on the reductive dechlorination of hexachloroethane by iron sulfide. Environ. Sci. Technol. 32: 1276-1284.

Caldwell, S. L., Laidler, J. R., Brewer, E. ., Eberly, J. O., Sandborgh, S. C., and Colwell, F. S., 2008. Anaerobic oxidation of methane: Mechanisms, bioenergetics, and the ecology of associated microorganisms. Environ. Sci. Technol. 42: 6791-6799.

Chen, M., Ma, L. Q. and Harris, W. G., 1999. Baseline Concentrations of 15 Trace Elements in Florida Surface Soils. J. Environ. Qual. 4: 1173-1181.

Cozzarelli, I. M., Herman, J. S., Baedecker, M. J. and Fischer, J. M., 1999. Geochemical heterogeneity of a gasoline-contaminated aquifer. J. Contam. Hydrol. 40(3): 261-284.

Cozzarelli, I. M., Suflita, J. M., Ulrich, G. A., Harris, S. H., Scholl, M. A., Schlottmann, J. L., and Christenson, S., 2000. Geochemical and microbiological methods for evaluating anaerobic processes in an aquifer contaminated by landfill leachate. Environ. Sci. Technol. 34: 4025-4033.

Cozzarelli, I. M., Schreiber, M. E., Erickson, M. L., and Ziegler, B. A., 2015. Arsenic cycling in hydrocarbon plumes: secondary effects of natural attenuation. GROUNDWATER. DOI: 10.1111/gwat.12316.

Crowe, S. A., Katsev, S., Leslie, K., Sturm, A., Magen, C., Nomosatryo, S., Pack, M. A., Kessler, J. D., Reeburgh, W. S., Roberts, J. A., Gonzalez, L., Haffner, G. D., Mucci, A., Sundby, B., and Fowle, D. A., 2011. The methane cycle in ferruginous Lake Matano. Geobiology 9: 61-78.

Curtis, G.P., 2003. Comparison of approaches for simulating reactive solute transport involving organic degradation reactions by multiple terminal electron acceptors. Computers and Geosciences 29: 319-329.

Davis, J. A. and Kent, D. B., 1990. Surface Complexation Modeling in Aqueous Geochemistry. *In:* M.F. Hochella and A.F. White (eds.), Mineral-Water Interface Geochemistry. Washington DC. Mineralogical Society of America, pp. 177-260.

Davis, J. A., Coston, J. A., Kent, D. B., and Fuller, C. C., 1998. Application of the surface complexation concept to complex mineral assemblages. Environ. Sci. Technol. 32: 2820-2828.

Dixit S. and Hering J. G., 2003. Comparison of Arsenic(V) and Arsenic(III) Sorption onto Iron Oxide Minerals: Implications for Arsenic Mobility. Environ. Sci. Technol. 37: 4182-4189.

Dzombak, D.A., and Morel, F.M.M., 1990. Surface Complexation Modeling: Hydrous Ferric Oxide, Wiley, New York, 393 p.

Essaid, H.I., Bekins, B.A., Herkelrath, W.N., Delin, G.N., 2011, Crude oil at the Bemidji Site - 25 years of monitoring, modeling, and understanding. Ground Water 49: 706–726. http://dx.doi.org/10.1111/j.1745-6584.2009.00654.x.

Ferry, M.L., R.T. Wilkin, R.G. Ford, J.T. Wilson, 2004. Nonbiological removal of *cis*-dichloroethylene in aquifer sediment containing magnetite. Environ. Sci. Technol. 38: 1746-1752.

Fischer, M. L., Bentley, A. J., Dunkin, K. A., Hodgson, A. T., Nazaroff, W. W., Sextro, R. G. and Daisey, J. M., 1996. Factors affecting indoor air concentrations of volatile organic compounds at a site of subsurface gasoline contamination. Environ. Sci. Technol. 30: 2948–2957.

Fredrickson J. K., Zachara, J. M., Kennedy, D. W., Dong, H., Onstott, T. C., Hinman, N. W. and Li, S., 1998. Biogenic iron mineralization accompanying dissimilatory reduction of hydrous ferric oxide by a groundwater bacterium. Geochim. Cosmochim. Acta 62: 3239-3257.

Grossman, E. L., Cifuentes, L. A. and Cozzarelli, I. M., 2002. Anaerobic methane oxidation in a landfill-leachate plume. Environ. Sci. Technol. 36: 2436-2442.

Guadalix M. E. and Pardo, M. T., 1991. Sulfate sorption by variable charge soils. J. Soil Sci. 42: 607-614.

Hansel, C. M., Benner, S. G. and Fendorf, S., 2005. Competing Fe(II)-induced mineralization pathways of ferrihydrite. Environ. Sci. Technol. 39: 7147-7153.

Harbaugh, A. W., 2005, MODFLOW-2005, the U.S. Geological Survey modular ground-water model – the Ground-Water Flow Process: U.S. Geological Survey Techniques and Methods, 6–A16.

He, Y., Su, C., Wilson, J., Wilkin, R., Adair, C., Lee, T., Bradley, P., Ferrey, M., 2009. Identification and characterization methods for reactive minerals responsible for natural attenuation of chlorinated organic compounds in ground water. EPA 600/R-09/115, December 2009.

He, Y. T., Fitzmaurice, A. G., Bilgin, A., Choi, S., O'Day, P., Horst, J, Harrington, J., Reisinger, H. J., Burris, D. R. and Hering, J. G., 2010. Geochemical processes controlling arsenic mobility in groundwater: A case study of arsenic mobilization and natural attenuation. Appl. Geochem. 25: 69–80.

Hering, J. G., O'Day, P. A., Ford, R. G., He, Y. T., Bilgin, A., Reisinger, H. J. and Burris, D. R., 2009. MNA as a remedy for arsenic mobilized by anthropogenic inputs of organic carbon. Ground Water Monit. Remed. 29: 84–92.

Hoelen, T. P. and Reinhard, M., 2004. Complete biological dehalogenation of chlorinated ethylenes in sulfate containing groundwater. Biodegradation 15: 395-403.

Höhn, R., Isenbeck-Schröter, M., Kent, D. B., Davis, J. A., Jakobsen, R., Jann, S., Niedan, V., Scholz, C., Stadler, S. and Tretner, A., 2006. Tracer test with As(V) under variable redox conditions controlling arsenic transport in the presence of elevated ferrous concentrations. J. Contam. Hydrol. 88: 36-54. doi:doi:10.1016/j.jconhyd.2006.06.001.

Hunter, K. L., Wang, Y., and van Cappellen, P., 1998, Kinetic modeling of microbially-driven redox chemistry of subsurface environments: coupling transport, microbial metabolism and geochemistry, J. Hydrol. 209: 53-80.

Jacob, C., Weber, E. F., Bet, J. N. and Macnair, A. K., 2005. Full-Scale Enhanced Reductive Dechlorination using Sodium Lactate and Vegetable Oil. *In:* B.C. Alleman and M.E. Kelley (Conference Chairs), Proceedings of the Eighth International *In Situ* and On-Site Bioremediation Symposium (Baltimore, Maryland; June 6-9, 2005), ISBN 1-57477-152-3, Battelle Press, Columbus, OH.

Jakobsen, R., Albrechtsen, H. J., Rasmussen, M., Bay, H., Bjerg, P. L.and Christensen, T. H., 1998. H-2 concentrations in a landfill leachate plume (Grindsted, Denmark): *In situ* energetics of terminal electron acceptor processes. Environ. Sci. Technol. 32: 2142-2148.

Jakobsen, R., and Postma, D., 1999. Redox zoning, rates of sulfate reduction and interactions with Fe-reduction and methanogenesis in a shallow sandy aquifer, Romo, Denmark, Geochim. Cosmochim. Acta 63: 137-151.

Keener, J., Borden, R. C., Lieberman, M. T., and Singletary, M. A., 2012. Pilot study to reduce sulfide toxicity in a TCE-contaminated aquifer undergoing enhanced reductive dechlorination. In: *Remediation of Chlorinated and Recalcitrant Compounds – 8th International Conference*, (Monterey, CA; May 2012), Battelle Press, Columbus, OH.

Kent, D. B. and Fox, P. M., 2004. The influence of groundwater chemistry on arsenic concentrations and speciation in a quartz sand and gravel aquifer. Geochem. Trans. 5: 1-12.

Kent, D. B., Wilkie, J. A. and J. A. Davis, 2007. Modeling the movement of a pH perturbation and its impact on adsorbed zinc and phosphate in a wastewater-contaminated aquifer. Water Resour. Res. 43, W07440. doi:10.1029/2005WR004841.

Kohler, M. and Kent, D. B., in prep., Modeling the impact of pH and dissolved salt concentrations on Zn, Ni and Pb sorption and transport in a quartz-sand aquifer, for submission to Geochim. Cosmochim. Acta.

Kouznetsova, I., Mao, X., Robinson, C., Barry, D. A., Gerhard, J. I., and McCarty P.L., 2010. Biological reduction of chlorinated solvents: Batch-scale geochemical modeling. Advances in Water Resources 33: 969-986.

Lee, W. and Batchelor, B., 2002. Abiotic Reductive Dechlorination of Chlorinated Ethylenes by Iron-Bearing Soil Minerals. 1. Pyrite and Magnetite. Environ. Sci. Technol. 36: 5147-5154.

Lee, W. and Batchelor, B., 2003. Reductive Capacity of Natural Reductants. Environ. Sci. Technol., 37: 535-541.

Löffler, F.E., Sanford, R.A. and Ritalahti, K.M., 2005. Enrichment, cultivation, and detection of reductively dechlorinating bacteria. Methods in Enzymology 397: 77-111.

Lovley, D. R. and Phillips, E. J. P., 1986. Organic Matter Mineralization with Reduction of Ferric Iron in Anaerobic Sediments. Appl. Environ. Microbiol. 51: 683–689

Lovley, D. R. and Phillips, E. J. P., 1987. Rapid Assay for Microbially Reducible Ferric Iron in Aquatic Sediments. Appl. Environ. Microbiol. 53: 1536–1540.

Ma, J., Rixey, W.G., DeVaull, G. E., Stafford, B. P. and Alvarez, P. J. J., 2012. Methane bioattenuation and implications for explosion risk reduction along the groundwater to soil surface pathway above a plume of dissolved ethanol. Environ. Sci. Technol. 46: 6013−6019.

Ng, G. H. C., Bekins, B. A., Cozzarelli, I. M., Baedecker, M. J., Bennett, P. C. and Amos, R. T., 2014. A mass balance approach to investigating geochemical controls on secondary water quality impacts at a crude oil spill site near Bemidji, MN. J. Contam. Hydrol. 164: 1-15. http://dx.doi.org/10.1016/j.jconhyd.2014.04.006.

Ng, G.-H.C., B.A. Bekins, I.M. Cozzarelli, M.J. Baedecker, P.C. Bennett, R.T. Amos, W.N. Herkelrath, 2015, Reactive transport modeling of geochemical controls on secondary water quality impacts at a crude oil spill site near Bemidji, MN, Water Resour. Res., 51, doi:10.1002/2015WR016964.

Ng, G. H., Kent, D. B., Kohler, M., LeBlanc, D. R., and Smith, R. L., (manuscript in co-author review), Geochemical modeling of sorption effects on aquifer re-oxygenation of a contaminant plume on Cape Cod, MA, for submission to Water Resour. Res.

Pierce, M. L. and Moore, C. B., 1982. Adsorption of arsenite and arsenate on amorphous iron hydroxide. Water Res. 16: 1247-1253.

Potsma, D. and Jakobsen, R., 1996. Redox Zonation: Equilibrium Constraints of the Fe(III)/SO4 Reduction Interface. Geochim. Cosmochim. Acta 60: 3169-3175.

Postma, D. and Appelo, C. A. J., 2000. Reduction of Mn-oxides by ferrous iron in a flow system: Column experiments and reactive transport modeling. Geochim. Cosmochim. Acta 64: 1237-1247.

Prommer, H., Barry, D.A. and Zheng, C., 2003, MODFLOW/MT3DMS-Based Reactive Multicomponent Transport Modeling, Groundwater, 41: 247–257. doi: 10.1111/j.1745-6584.2003.tb02588.x

Raghoebarsing, A. A., Pol, A., van de Pas-Schoonen, K. T., Smolders, A. J. P., Ettwig, K. F., Rijpstra, W. I. C., Schouten, S., Damste, J. S. S., Op den Camp, H. J. M., Jetten, M. S. M. and Strous, M., 2006. A microbial consortium couples anaerobic methane oxidation to denitrification. Nature 440(7086): 918-921.

Repert, D.A., Barber, L.B., Hess, K.M., Keefe, S.H., Kent, D.B., Leblanc, D.R., Smith, R.L., 2006. Long-term natural attenuation of carbon and nitrogen within a groundwater plume after removal of the treated wastewater source. Environ. Sci. Technol. 40: 1154-1162.

Riis, C., Christensen, A. G., Nielsen, H. H., Van Bemmel, M. and Ostergaard, 2007. Long-term Bioremediation of a Chlorinated Solvents Plume in a Fractured Limestone Aquifer Using a Dechlorinating Bioreactor. *In:* Proceedings of the Ninth International *In Situ* and On-Site Bioremediation Symposium (Baltimore, MD; May 2007), Battelle Press, Columbus, OH.

Roden, E. E. and Zachara, J. M., 1996. Microbial reduction of crystalline iron(III) oxides: influence of oxide surface area and potential for cell growth. Environ. Sci. Technol. 30: 1618–1628.

Roden, E. E., Urrutia, M. M. and Mann, C. J., 2000. Bacterial reductive dissolution of crystalline Fe(III) Oxide in continuous-flow column reactors. Appl. Environ. Microbiol. 66: 1062–1065.

Roden, E .E. and Urrutia, M. M., 2002. Influence of biogenic Fe(II) on bacterial reduction of crystalline Fe(III) oxides. Geomicrobiology J. 19: 209–251.

Schirmer, M., Durrant, G. C., Molson, J. W., and Frind, E. O., 2001. Influence of transient flow on contaminant biodegradation. Ground Water 39: 276-282.

Sihota, N. J., Mayer, K. U., Toso, M. A. and Atwater, J. F., 2013. Methane emissions and contaminant degradation rates at sites affected by accidental releases of denatured fuel-grade ethanol. J. Contam. Hydrol. 151: 1-15.

Sleep, B. E., Brown, A. J., and Lollar, B. S., 2005. Long-term tetrachloroethene degradation sustained by endogenous cell decay. J. Environ. Eng. Sci. 4: 11-17.

Smedley, P. L. and Kinniburgh, D. G., 2002. A Review of the Source, Behaviour and Distribution of Arsenic in Natural Waters. Appl. Geochem. 17: 517-568.

Smith, R. L., Repert, D. A., Barber, L. B., and LeBlanc, D. R., 2013, Long-term groundwater contamination after source removal – The role of sorbed carbon and nitrogen on the rate of reoxygenation of a treated-wastewater plume on Cape Cod, MA, USA, Chem. Geol. 337-338: 38-47.

Sung, Y., 2005. Isolation and ecology of bacterial populations involved in reductive dechlorination of chlorinated solvents. Ph.D. Dissertation, Georgia Institute of Technology, Atlanta, GA.

Tebo, B. M., Bargar, J. R., Clement, B. G., Dick, G. J., Murray, K. J., Parker, D., Verity, R. and Webb, S. M., 2004. Biogenic manganese oxides: properties and mechanisms of formation. Ann. Rev. Earth Planet. Sci. 32: 287-328.

Thorn, K.A., and G.R. Aiken, 1998, Biodegradation of crude oil into nonvolatile organic acids in a contaminated aquifer near Bemidji, Minnesota, Org. Geochem. 29: 909–931.

TSI and Solutions-IES, 2003. Interim Report: Technology Application of Low Cost Emplacement of Insoluble Organic Substrate for Enhanced *In Situ* Reductive Dechlorination of Halogenated Aliphatic Hydrocarbons, Dover Air Force Base. Prepared for the Air Force Center for Environmental Excellence, Brooks City-Base, TX. March.

United States Environmental Protection Agency (USEPA), 2009. List of Drinking Water Contaminants and Their MCLs. U.S. Environmental Protection Agency, Washington DC (http://www.epa.gov/safewater/contaminants/index.html).

USEPA, 2010. *Integrated Risk Information System, Hydrogen Sulfide* (CASRN 7783). U.S. Environmental Protection Agency, Washington, DC (http://www.epa.gov/IRIS/subst/0061.htm).

USEPA, 2013. Five-Year Review Report, Grants Chlorinated Solvent Plume Superfund Site. U.S. Environmental Protection Agency, Washington, DC (http://www.epa.gov/region6/6sf/newmexico/grants/nm_grants_5yr_review_9-13.pdf.).

Vanbroekhoven, K., Satyawali, Y., Van Roy, S., Vangeel, S., Gemoets, J., Muguet, S., Zeuwts, L., Gommers, K. and Feyaerts, K., 2009. Stability of Metal Precipitates Formed after *In Situ* Bioprecipitation Induced by Sulfidogenesis. *In:* Proceedings of the Tenth International *In Situ* and On-Site Bioremediation Symposium (Baltimore, MD; May 5-8, 2009), Battelle Press, Columbus, OH.

Villalobos, M., Toner, B., Bargar, J. and Sposito, G., 2003. Characterization of the manganese oxide produced by *Pseudomonas putida* strain MnB1. Geochim. Cosmochim. Acta 67: 2649-2662.

Warren, E., Sihota, N. J., Hosterrler, F. D. and Bekins, B. A., 2014. Comparison of surficial CO_2 efflux to other measures of subsurface crude oil degradation. J. Contam. Hydrol. 164: 275-284.

Wielinga, B., Bostick, B., Hansel, C. M., Rosenzweig, R. F. and Fendorf, S., 2000. Inhibition of Bacterially Promotoed Uranium Reduction: Ferric (Hydr)oxides as Competitive Electron Acceptors. Environ. Sci. Technol. 34 (11): 2190-2195.

Yurovsky, M., Cacciatore, D., Hudson, L., Leigh, D. P., Bhullar, C. and Shaheen, W., 2009. Operation of *In Situ* System for Treatment of Hexavalent Chromium at the Selma Pressure Treating Superfund Site. *In:* Proceedings of the Tenth International *In Situ* and On-Site Bioremediation Symposium (Baltimore, MD; May 2009), Battelle Press, Columbus, OH.

APPENDIX A

DATABASE TABLES

Table A-1. Characteristics of ERB Sites Included in SWQI Database.

Site ID	Location	Injection Type	Organic Substrate	Data Source	No. of wells	Record (months)
Aerojet General Corporation	Rancho Cordova, CA	Horizontal Wells	Citric Acid	ESTCP Project Report	18	24
Aiea Laundry	Pearl Harbor, HI	Source	EOS, Lactate	Personal Correspondence	2	6
Altus AFB OU1 - Biowall	Altus, OK	Biowall	Mulch and compost	AFCEE Project Report	44	88
Altus AFB OU1 - Injections	Altus, OK	Source	EVO	Monitoring Report	5	20
Altus AFB SS-17	Altus, OK	PRB	EVO	Monitoring Report	14	20
Altus AFB SS-18	Altus, OK	Source	EOS	Monitoring Report	22	21
Altus AFB SS-22	Altus, OK	Source	EOS	Monitoring Report	52	21
Avon Park AFB	Avon Park, FL	Recirc	Lactate, ethanol	SERDP Project Report	5	5
Beale AFB Site 39 Building 2145	Marysville, CA	Source	EOS	Monitoring Report	9	15
Beale AFB Site 39 Source Area 1	Marysville, CA	Source	EOS	Monitoring Report	18	10
Boeing Former Compton Site	Compton, CA	Source	Newman Zone	Monitoring Report	14	36
Cape Canaveral Hangar K	Cape Canaveral, FL	Source	Soybean oil	AFCEE Project Report	19	68
Charleston NWS SWMU 17	Charleston, SC	Source	EOS	ESTCP Project Report	26	41
Cornhusker AAP OU1	Grand Island, NE	PRB	Newman Zone, Wesblend 66	Monitoring Report	47	48
Crown Cork & Seal Facility	Pittsburg, CA	Source	HRC	Monitoring Report	2	66
Dover AFB Area 5	Dover, DE	PRB	Lactate, Newman Zone	Monitoring Report	43	77
Dover AFB Area 6	Dover, DE	PRB	Lactate, Newman Zone	Monitoring Report	136	77
Dover AFB Site WP14	Dover, DE	Biowall	Mulch	AFCEE Project Report	14	39
East Charleston Business Park	Mountain View, CA	PRB	HRC	Monitoring Report	9	64
Fort Devens AOC 50	Devens, MA	PRB	Molasses	Monitoring Report	9	30
Fort Dix MAG-1	Fort Dix, NJ	Recirc	Lactate	ESTCP Project Report	22	12
Fort Worth Joint Reserve Base AOC-2	Fort Worth, TX	PRB	Soybean oil and HF corn syrup	AFCEE Project Report	14	26
Hickam AFB Site LF05 - Southeast Area	Honolulu, HI	Recirc	Lactic acid	Monitoring Report	37	4
Hickam AFB Site LF05 - TCRA Area	Honolulu, HI	PRB	Soybean oil	AFCEE Project Report	11	26
Indian Head Naval Surface Warfare Center	Indian Head, MD	Recirc	Lactic acid	Literature Report	14	5
JEB Little Creek Site 11	Virginia Beach, VA	PRB	SRS emulsified oil	Monitoring Report	26	12
JEB Little Creek Site 12	Virginia Beach, VA	PRB	EOS	Monitoring Report	17	13
JEB Little Creek Site 13	Virginia Beach, VA	PRB	LactOil, ethyl lactate	Monitoring Report	28	6

Site ID	Location	Injection Type	Organic Substrate	Data Source	No. of wells	Data Record (months)
Maryland Perchlorate Site	Elkton, MD	PRB	EOS	ESTCP Project Report	8	42
McConnell AFB Site FT07	Wichita, KS	Biowall/Recirc	Mulch and soybean oil	Monitoring Report	18	8
Mercedes North Houston	Houston, TX	Source	HRC, Newman Zone, Cheese Whey	Monitoring Report	10	51
Moffett Field Site 26	Mountain View, CA	Source	EHC	Monitoring Report	14	22
Moffett Field Site 28 - Building 88	Mountain View, CA	Source	Lactate and lactic acid	Monitoring Report	7	10
Moffett Field Site 28 - Traffic Island	Mountain View, CA	Source	Lactoil	Monitoring Report	6	10
Moffett Field Site 28 - W9-18 Area	Mountain View, CA	Source	EHC	Monitoring Report	12	10
Naval Weapons Station Seal Beach - Site 40	Seal Beach, CA	Source	Sodium lactate, HRC	Monitoring Report	7	75
Oates Park	Mesquite, TX	Source	HRC	Monitoring Report	34	36
Pacific Scientific	Santa Barbara, CA	Source	HRC	Monitoring Report	4	110
Picatinny Arsenal Area 157	Dover, NJ	Recirc	Cheese whey	ESTCP Project Report	14	18
Renco Encoders	Goleta, CA	Source, PRB	HRC, HRC-X, Wilclear, Lactoil, EOS, EHC	Monitoring Report	14	117
Savannah River Site - F Area	Aiken, SC	Source	Molasses	Monitoring Report	27	19
Tinker AFB FTA-2	Oklahoma City, OK	Source	Soybean oil and HF corn syrup	AFCEE Project Report	20	23
Travis AFB Site DP039	Fairfield, CA	Biowall/Recirc	Mulch and soybean oil	Monitoring Report	10	11
Treasure Island Site 24	San Francisco, CA	Recirc	Sodium lactate	Monitoring Report	9	12
TRW Microwave	Santa Clara, CA	Source, PRB	HRC, Cheese Whey, EVO, EHC-L, ABC[+]	Monitoring Report	20	132
Western Microwave	Sunnyvale, CA	PRB	HRC	Monitoring Report	33	68
Whittaker Bermite Facility Area	Santa Clarita, CA	Recirc	Citric Acid	Monitoring Report	13	7

Notes
PRB - Permeable reactive barrier
Recirc - Recirculation system
Source - Source area injections

Table A-2. Summary Statistics for Post-Injection Data Contained in SWQI Database.

	Well Location	Monitoring Points	Percentiles						
			Min	10th	25th	50th	75th	90th	Max
Maximum Total Organic Carbon (mg/L)	Upgradient	113	<1	1.4	2.3	3.8	12	38	258
	Injection Area	303	0.3	3.1	12	230	1,038	3,548	33,000
	0-10 m Downgradient	174	<1	3.2	10	57	263	738	7,890
	10-25 m Downgradient	64	<1	1.9	2.8	7.0	81	385	5,080
	25-50 m Downgradient	35	<1	1.6	<5	9.6	20	125	885
	50+ m Downgradient	75	0.833	2.2	3.0	5.7	15	28	864
Maximum Dissolved Manganese (mg/L)	Upgradient	61	0.002	0.0066	0.057	0.2	0.53	1.1	39
	Injection Area	125	0.023	0.15	0.80	2.6	8.7	17	53
	0-10 m Downgradient	112	0.0065	0.018	0.087	1.1	4.5	12	86
	10-25 m Downgradient	52	0.0015	0.020	0.13	0.44	1.7	7.1	59
	25-50 m Downgradient	20	0.002	0.010	0.024	0.077	0.20	0.97	2.0
	50+ m Downgradient	17	0.006	0.018	0.042	0.2	3.2	15	31
Maximum Dissolved Iron (mg/L)	Upgradient	109	<0.04	<0.1	0.1	0.43	1.1	6.0	350
	Injection Area	203	0.02	0.14	2.0	22	120	266	1,200
	0-10 m Downgradient	180	0.02	0.16	1.2	8.2	78	251	928
	10-25 m Downgradient	64	<0.1	0.17	0.50	6.9	50	218	470
	25-50 m Downgradient	33	<0.1	0.38	1	8.9	75	167	404
	50+ m Downgradient	69	0.01	0.1	0.2	0.74	5	21	200
Maximum Dissolved Arsenic (mg/L)	Upgradient	39	<0.00031	0.00031	0.0016	0.0035	0.005	0.012	0.073
	Injection Area	44	0.0011	<0.01	0.0088	0.033	0.11	0.49	1.2
	0-10 m Downgradient	60	0.0011	0.0028	<0.01	0.014	0.040	0.096	0.90
	10-25 m Downgradient	18	0.0012	0.0040	<0.012	0.011	0.042	0.36	0.75
	25-50 m Downgradient	6	<0.005	<0.0075	<0.01	0.0056	0.022	0.029	0.032
	50+ m Downgradient	10	<0.005	<0.005	<0.005	0.0056	0.06768	0.111	0.12
Minimum Sulfate (mg/L)	Upgradient	124	<0.1	4.5	14	81	281	1,285	1,870
	Injection Area	300	<0.1	0.36	1	9.7	81	450	3,150
	0-10 m Downgradient	222	<0.2	<0.5	<0.2	8.5	98	843	3,100
	10-25 m Downgradient	78	0.12	0.49	1.5	13	96	643	2,930
	25-50 m Downgradient	36	0.1	<0.5	0.70	11	120	210	2,900
	50+ m Downgradient	75	0.1	0.37	1	13	120	416	2,400
Maximum Sulfide (mg/L)	Upgradient	59	0.0215	<0.05	0.0745	<1	0.575	2.32	190
	Injection Area	119	<0.05	0.256	0.78	2	10	110.2	344
	0-10 m Downgradient	86	0.01	0.086	0.39375	1.06	2.21	9.55	1300
	10-25 m Downgradient	38	<0.04	<0.1	0.4025	0.88	2.535	8.144	20
	25-50 m Downgradient	21	<0.05	<0.1	0.3	<1	0.9	1.3	1.6
	50+ m Downgradient	15	<0.1	<1	0.6	<2	1.75	2.54	2.9
Maximum Methane (mg/L)	Upgradient	107	0.0001	0.0015	0.0029	0.063	0.32	1.3	6.2
	Injection Area	261	<0.00031	0.050	1.2	9.0	15	23	120
	0-10 m Downgradient	197	0.0028	0.20	0.91	7.6	17	31	77
	10-25 m Downgradient	69	0.00037	0.0056	<0.025	1.9	11	28	56
	25-50 m Downgradient	36	0.0002	0.0045	0.059	1.9	17	24	40
	50+ m Downgradient	74	0.00022	<0.002	0.013	0.25	4.9	17	35

Table A-2 (continued). Summary Statistics for Post-Injection Data Contained in SWQI Database.

	Well Location	Monitoring Points	Percentiles						
			Min	10th	25th	50th	75th	90th	Max
Minimum Dissolved Oxygen (mg/L)	Upgradient	130	0	0	0.02	0.32	1.4	2.9	7.3
	Injection Area	323	0	0	0.05	0.15	0.45	1.1	8.8
	0-10 m Downgradient	208	0	0	0	0.07	0.2	1.3	10
	10-25 m Downgradient	81	0	0	0.04	0.18	0.81	1.8	6.1
	25-50 m Downgradient	39	0	0	0.01	0.11	0.28	0.60	1.4
	50+ m Downgradient	79	0	0.07	0.12	0.2	0.46	1.6	9.4
Minimum Nitrate (mg/L as N)	Upgradient	73	0.0011	0.028	<0.1	<0.22	1.7	4.8	12
	Injection Area	136	<0.0066	0.0058	<0.05	<0.11	0.19	0.59	14
	0-10 m Downgradient	132	0.00068	0.0055	<0.05	<0.2	0.20	0.41	3.5
	10-25 m Downgradient	45	<0.01	<0.01	<0.05	<0.2	0.90	6.2	25
	25-50 m Downgradient	16	<0.01	<0.01	<0.01	0.075	0.51	2.2	2.5
	50+ m Downgradient	21	<0.01	<0.05	<0.11	0.16	1.3	2.5	5.9
Median pH (Non-Buffered) (SU)	Upgradient	106	3.9	5.8	6.6	6.8	7.1	7.2	11.7
	Injection Area	223	4.9	5.7	6.2	6.6	6.8	7.2	8.7
	0-10 m Downgradient	132	4.8	6.1	6.4	6.7	7.0	7.2	8.4
	10-25 m Downgradient	55	4.9	6.3	6.7	7.0	7.2	7.5	10.0
	25-50 m Downgradient	16	6.1	6.6	6.8	7.0	7.2	7.6	7.7
	50+ m Downgradient	46	5.8	6.2	6.6	6.9	7.1	7.2	9.4
Median pH (Buffered) (SU)	Upgradient	41	3.6	4.6	4.8	5.4	5.9	6.6	7.2
	Injection Area	106	4.2	4.9	5.3	6.0	6.5	6.8	8.9
	0-10 m Downgradient	86	3.5	5.4	5.8	6.1	6.5	6.9	10.3
	10-25 m Downgradient	25	3.8	5.1	5.9	6.1	6.5	6.8	11.2
	25-50 m Downgradient	23	4.7	5.1	5.3	5.8	6.2	6.5	7.7
	50+ m Downgradient	32	3.7	4.8	4.9	5.1	5.4	6.4	8.2
Median ΔpH (Non-Buffered) (S.U.)	Upgradient	76	-1.9	-0.90	-0.32	-0.12	0.02	0.25	1.2
	Injection Area	165	-3.3	-1.6	-0.90	-0.35	0.00	0.31	1.4
	0-10 m Downgradient	108	-3.8	-1.2	-0.54	-0.21	0.15	0.63	1.0
	10-25 m Downgradient	47	-3.2	-1.2	-0.58	-0.20	0.01	0.19	2.7
	25-50 m Downgradient	9	-0.68	-0.49	-0.39	-0.21	0.00	0.11	0.38
	50+ m Downgradient	34	-1.6	-0.33	-0.17	-0.10	0.02	0.07	0.24
Median ΔpH (Buffered) (S.U.)	Upgradient	35	-0.90	-0.42	-0.20	0.10	0.44	0.81	1.4
	Injection Area	57	-2.0	-1.3	-0.4	0.4	1.3	2.1	4.4
	0-10 m Downgradient	73	-2.9	-0.13	0.19	0.47	1.0	1.6	3.7
	10-25 m Downgradient	16	-2.8	-1.2	-0.09	0.60	1.5	1.9	2.6
	25-50 m Downgradient	21	-1.3	-0.81	-0.27	0.12	0.59	0.84	2.1
	50+ m Downgradient	24	-1.0	-0.51	-0.18	-0.01	0.12	0.46	0.86
Minimum ΔORP (mV)	Upgradient	87	-665	-402	-280	-187	-83	-22	52
	Injection Area	193	-870	-492	-364	-254	-138	-53	27
	0-10 m Downgradient	160	-936	-463	-353	-269	-168	-95	-1
	10-25 m Downgradient	58	-848	-466	-334	-263	-123	-56	0
	25-50 m Downgradient	23	-660	-451	-422	-289	-223	-60	-8
	50+ m Downgradient	45	-491	-362	-302	-219	-73	-33	-7

Notes

mg/L   Milligrams per liter
S.U.   Standard Units
mV   Millivolts

APPENDIX B
SCIENTIFIC AND TECHNICAL PUBLICATIONS

Journal Articles

Amos, R. T., B. A. Bekins, G. N. Delin, I. M. Cozzarelli, D. W. Blowes, and J. D. Kirshtein, 2011, Methane oxidation in a crude oil contaminated aquifer: Delineation of aerobic reactions at the plume fringes, Journal of Contaminant Hydrology, doi:10.1016/j.jconhyd.2011.04.003.

Baedecker, M.J., R. P. Eganhouse, B.A. Bekins, G.N. Delin, 2011, Loss of volatile hydrocarbons from an LNAPL oil source, Journal of Contaminant Hydrology, doi: 10.1016/j.jconhyd.2011.06.006.

Bekins, B. A., M.J. Baedecker, R.P. Eganhouse, and W. N. Herkelrath, 2011, Long-term natural attenuation of crude oil in the subsurface, in Groundwater Quality: Management in a Rapidly Changing World, E. Hoehn and M. Schirmer (eds.), International Association of Hydrological Sciences Publication 342, p. 123-127.

Amos, R. T., B. A. Bekins, I. M. Cozzarelli, M. A. Voytek, J. D. Kirshtein, E. J. P. Jones and D. W. Blowes, 2012, Evidence for iron-mediated anaerobic methane oxidation in a crude oil-contaminated aquifer, Geobiology, DOI: 10.1111/j.1472-4669.2012.00341.x

Rasa, E., B. A. Bekins, D. M. Mackay, N. R. de Sieyes, J. T. Wilson, K. P. Feris, I. A. Wood, K. M. Scow, 2013, Impacts of ethanol-blended fuels release on groundwater aquifers and fate of produced methane: Simulation of field observations, Water Resources Research, 8:4907-4926, doi:10.1002/wrcr.20382.

Ng, G.-H.C., B.A. Bekins, I.M. Cozzarelli, M.J. Baedecker, P.C. Bennett, and R.T. Amos, 2014, A mass balance approach to investigating geochemical controls on secondary water quality impacts at a crude oil spill site near Bemidji, MN, Journal of Contaminant Hydrology, 164:1-15, doi:10.1016/j.jconhyd.2014.04.006.

Hiortdah, K. M., and R. C. Borden, Enhanced reductive dechlorination of tetrachloroethene dense non-aqueous phase liquid with EVO and $Mg(OH)_2$, 2014, Environmental Science & Technology, 48:624−631, doi:10.1021/es4042379.

Essaid, H.I., B.A. Bekins, I.M. Cozzarelli, 2015, Organic contaminant transport and fate in the subsurface: Evolution of knowledge and understanding, Water Resources Research, 51:4861-4902, doi:10.1002/2015WR017121.

Ng, G.-H.C., B.A. Bekins, I.M. Cozzarelli, M.J. Baedecker, P.C. Bennett, R.T. Amos, and W.N. Herkelrath, 2015, Reactive transport modeling of geochemical controls on secondary water quality impacts at a crude oil spill site near Bemidji, MN, Water Resources Research, 51:4156–4183, doi:10.1002/2015WR016964.

Tillotson, J. M. and R. C. Borden, Secondary Water Quality Impacts Due to Enhanced Reductive Bioremediation: A Statistical Summary of 47 Sites, Groundwater Monitoring and Remediation, In Press Sept 2015.

Tillotson, J. M. and R. C. Borden, Comparison of Chlorinated Ethene Degradation Rates and Geochemical Conditions at 43 Enhanced Reductive Bioremediation Sites, Journal of Contaminant Hydrology, In preparation.

Ng, G.-H.C., D.B. Kent, M. Kohler, D. LeBlanc, and R. Smith, Geochemical modeling of sorption effects on aquifer re-oxygenation in Cape Cod, MA, In preparation.

Kohler, M. and D. B. Kent, Modeling the impact of pH and dissolved salt concentration on the sorption of nickel, zinc, and lead on an aquifer sediment, In preparation.

Technical Reports

Borden, R. C., Tillotson, J. M., Ng, G.-H. C., Bekins, B. A., Kent, D. B., and Curtis, G. P., 2015. Extent and Persistence of Secondary Water Quality Impacts after Enhanced Reductive Bioremediation. Strategic Environmental Research and Development Program, Arlington, VA, www.serdp-estcp.org.

Borden, R. C., Tillotson, J. M., Ng, G.-H. C., Bekins, B. A., Kent, D. B., and Curtis, G. P., 2016. Impacts of Enhanced Reductive Bioremediation on Post-Remediation Groundwater Quality, ER-2131, FINAL REPORT, Strategic Environmental Research and Development Program, Arlington, VA, www.serdp-estcp.org.

Conference Presentations and Posters

Tillotson, J. M., R. C. Borden, B. A. Bekins, D. B. Kent, and G. P. Curtis, 2011. Post-Remediation Water Quality Impacts of Enhanced Reductive Dechlorination (2131), Partners in Environmental Technology Symposium & Workshop, Washington, DC, (poster).

Bekins, B.A., M.J. Baedecker, R.P. Eganhouse, D. W.N. Herkelrath, E. Warren, I.M. Cozzarelli, 2011, Hydrologic Controls on Losses of Individual Components of Crude Oil in the Subsurface AGU, Fall Meet. Suppl, H41A-1006 (poster)

Tillotson, J. M., R. C. Borden, 2012. Statistical Evaluation of Post-Remediation Impacts at Anaerobic Bioremediation Treatment Sites, Remediation of Chlorinated and Recalcitrant Compounds – 8th Internat. Conf., May 2012, Monterey, CA.

Ng, G. C., B. A. Bekins, I.M. Cozzarelli; M.J. Baedecker; R. T. Amos, Reactive transport modeling of long-term secondary water quality impacts of a crude oil spill at Bemidji, Minnesota, Abstract H43E-1403, AGU Fall Meeting, 3-7 Dec., 2012, San Francisco, Calif.

Kent, D. B.; Kohler, M.; Curtis, G. P.; Fairchild, G. M.; LeBlanc, D. R., Modeling the impact of variable pH and dissolved salt concentrations on metal ion transport observed in field experiments, 22nd Goldshmidt Conference, June 24-29, 2012, Montreal, Quebec, Canada (invited presentation)

Tillotson, J. M., R. C. Borden, 2013. Post-Remediation Metals Mobilization Following Enhanced Anaerobic Bioremediation, 2nd International Symposium on Bioremediation and Sustainable Environmental Technologies, June 10-13, 2013, Jacksonville, Florida.

Ng, G.-H.C., J. Tillotson, B.A. Bekins, and D.B. Kent, 2013. A cross-site study of processes controlling secondary water quality impacts of anaerobic biodegradation, GSA Annual Meeting, Denver, CO, October 29, 2013.

Book Chapters

Rifai, H.S., R. C. Borden, C. J. Newell, and P. B. Bedient, Modeling Remediation of Chlorinated Solvent Plumes, In Situ Remediation of Dissolved Chlorinated Solvent Plumes, Ed. H.F. Stroo and C.H. Ward, Springer, New York, NY, pp. 145-184, 2011.

Heiderscheidt, J.L., T.H. Illangasekare, R.C. Borden, N.R. Thomson, Principles of ISCO Transport and Modeling, In Situ Chemical Oxidation for Remediation of Contaminated Groundwater, Ed. R Siegrist, M Crimi, and T Simpkin Springer, New York, NY, pp. 233-284, 2012.

Lai, Y., Borden, R.C., Alperin, E., Physical-Chemical Treatment of Metals and Radionuclides in the Saturated Zone using Colloidal Buffers, Waste Management 2012 Conference, February 26 – March 1, 2012, Phoenix, AZ.

Stroo, H.F., M.R. West, B.H. Kueper, R.C. Borden, C.H. Ward, In Situ Bioremediation of Chlorinated Ethene Source Zones, Chlorinated Solvent Source Zone Remediation, Ed. B.H. Kueper, H.F. Stroo and C.H. Ward, Springer, New York, NY, 2014.